Spiral anchoring in media with multiple inhomogeneities: a dynamical system approach

P Boily‡, V G LeBlanc and E Matsui

Department of Mathematics and Statistics, University of Ottawa, Ottawa K1N 6N5, Canada

E-mail: `pboily@uottawa.ca`

Abstract. The spiral is one of Nature's more ubiquitous shape: it can be seen in various media, from galactic geometry to cardiac tissue. In the literature, very specific models are used to explain some of the observed incarnations of these dynamic entities. Barkley [1, 2] first noticed that the range of possible spiral behaviour is caused by the Euclidean symmetry that these models possess.

In experiments however, the physical domain is never perfectly Euclidean. The heart, for instance, is finite, anisotropic and littered with inhomogeneities. To capture this loss of symmetry (and as a result model the physical situation with a higher degree of accuracy), LeBlanc and Wulff introduced forced Euclidean symmetry-breaking (FESB) in the analysis, *via* two basic types of perturbations: translational symmetry-breaking (TSB) and rotational symmetry-breaking terms. In [3, 4], they show that phenomena such as anchoring and quasi-periodic meandering can be explained by combining Barkley's insight with FESB.

In this article, we provide a fuller characterization of spiral anchoring by studying the effects of n simultaneous TSB perturbations, where $n > 1$.

AMS classification scheme numbers: 34C20, 37G40, 37L10, 37N25, 92E20

‡ Present address: Institute of the Environment, University of Ottawa, Ottawa K1N 6N5, Canada.

arXiv:math/0512511v2 [math.DS] 19 Jan 2006

1. Introduction

Spiral waves have been observed in a variety of experimental contexts, ranging from the well-known Belousov-Zhabotinsky chemical reaction to the electrical potential in cardiac tissue [1, 2, 5–16]. In this last case, spiral waves are believed to be a precursor to several fatal cardiac arrythmias (*e.g.* ventricular tachycardia and ventricular fibrillation) [13, 17, 18]. A thorough understanding of the various dynamical properties of spiral waves is therefore warranted.

One of the most interesting and fruitful approaches in recent years to the study of spiral waves has been to use the theory of equivariant dynamical systems to derive finite-dimensional models for many of the observed dynamical states and bifurcations of spirals. The pioneer of this approach was Barkley, who realized that the experimentally-observed transition from rigid rotation to quasi-periodic meandering and drifting could be explained using only the underlying symmetries (the group $\mathbb{SE}(2)$ of all planar translations and rotations) of the governing reaction-diffusion partial differential equations: he derived an *ad hoc* system of 5 ordinary differential equations with $\mathbb{SE}(2)$ symmetry which model a Hopf bifurcation from a rotating wave, and then showed that this finite-dimensional system replicated the experimentally-observed transition to meandering and drifting [1, 2, 19]. Sandstede, Scheel and Wulff later proved a general center manifold reduction theorem for relative equilibria and relative periodic solutions in spatially extended infinite-dimensional $\mathbb{SE}(2)$-equivariant dynamical systems, thereby providing mathematical justification for Barkley's approach [20–24].

One of the advantages of this equivariant dynamical systems approach is that one can often give universal, model-independent explanations of many of the observed dynamics and bifurcations of spiral waves. For example, the above-mentioned Hopf bifurcation from rigid rotation to quasi-periodic meandering and drifting has been observed in both numerical simulations [16] and in actual chemical reactions [5]. Another example is the anchoring/repelling of spiral waves on/from a site of inhomogeneity, which has been observed in numerical integrations of an Oregonator system [8], in photo-sensitive chemical reactions [7] and in cardiac tissue [11]. Using a model-independent approach based on forced symmetry-breaking, LeBlanc and Wulff showed that anchoring/repelling of rotating waves is a generic property of systems in which the translation symmetry of $\mathbb{SE}(2)$ is broken by a small perturbation [3]. Similarly, some dynamics of spiral waves observed in anisotropic media (*e.g.* phase-locking and/or linear drifting of meandering spiral waves) have been shown to be generic consequences of rotational symmetry-breaking [4, 12, 25–28].

Consider as a paradigm a system of reaction-diffusion partial differential equations

$$\frac{\partial u}{\partial t} = D \cdot \nabla^2 u + f(u) \tag{1.1}$$

where u is a k-vector valued function of time and two-dimensional space, D is a matrix of diffusion coefficients and $f : \mathbb{R}^k \longrightarrow \mathbb{R}^k$ is a smooth reaction term. Many of the phenomena in which spiral waves are observed experimentally are modeled by systems of the form (1.1). Moreover, Scheel has proved that systems of this form can admit time-periodic, rigidly rotating spiral wave solutions [29]. Implicit in the form of equations (1.1) is the fact that the medium of propagation is completely homogeneous and isotropic. Mathematically, this is represented by the invariance of (1.1) under the transformations

$$u(t, x) \longmapsto u(t, x_1 \cos\theta - x_2 \sin\theta + p_1, x_1 \sin\theta + x_2 \cos\theta + p_2), \qquad (1.2)$$

where $(\theta, p_1, p_2) \in \mathbb{S}^1 \times \mathbb{R}^2$ and $x \in \mathbb{R}^2$ [30, 31]. The group of all transformations of the form (1.2) is isomorphic to the special Euclidean group $\mathbb{SE}(2)$ of all planar translations and rotations.

When studying the effects of inhomogeneities on the propagation of spiral waves, one must consider a larger class of models than (1.1), since inhomogeneous media do not possess Euclidean invariance. For example, one might consider systems of the form

$$\frac{\partial u}{\partial t} = D \cdot \nabla^2 u + f(u) + \lambda \, g(u, \|x\|^2, \lambda) \qquad (1.3)$$

which are perturbations of (1.1). Such systems could model a spatially extended reaction-diffusion medium in which there is one site of inhomogeneity (with circular symmetry) centered at the origin of $\mathbb{R}^2$. For instance, the Oregonator model which is used to study spiral anchoring in [8] is of the form (1.3). When $\lambda \neq 0$, (1.3) has rotational symmetry about the origin, but does not possess any translation symmetry. This phenomenon is called *forced translational symmetry-breaking*; it is studied in detail in [3].

In this paper, we use a similar equivariant dynamical systems approach to study the problem of spiral wave dynamics (specifically, with regards to anchoring/repelling) in media in which there are several sites of inhomogeneities (as opposed to just one site), of which cardiac tissue is an important example.

We will make several simplifying assumptions which are meant to make the analysis more tractable. First, we assume that the inhomogeneities consist of a finite number of "sources" which are localized near distinct sites $\zeta_1, \ldots, \zeta_n$ in the plane. Second, we will assume that these n sources of inhomogeneity are independent in the following sense: we introduce n independent real parameters $\lambda_1, \ldots, \lambda_n$ which give some measure of the relative "amplitudes" of the sources. In particular, when all the λ_i are zero except, say $\lambda_{i*} \neq 0$, then there is only one source of inhomogeneity localized near the point ζ_{i*}. In that case, we will make a third simplifying assumption: the single inhomogeneity is circularly symmetric around the point ζ_{i*}. The following is an example of a class

of reaction-diffusion partial differential equations which are perturbations of (1.1) and which might model such a situation:

$$u_t = \tilde{D}\Delta u + f(u) + \sum_{j=1}^{n} \lambda_j \left[\hat{D}_j(\|x - \zeta_j\|^2, \lambda)\Delta u + f_j(u, \|x - \zeta_j\|^2, \lambda) \right], \qquad (1.4)$$

where the functions $\hat{D}_j, f_j$ are bounded and smooth enough. The goal of this paper is to provide a detailed analysis of a larger class of abstract dynamical systems which share the symmetry properties of (1.4):

(S1) when $\lambda_1 = \cdots = \lambda_n = 0$, the systems are invariant under the action (1.2) of the group $\mathbb{SE}(2)$,

(S2) when all the λ_i are zero except λ_{i*}, the systems have rotational symmetry about the point ζ_{i*}, but they do not generically possess translation symmetries,

(S3) when two or more of the λ_i are non-zero, the systems do not generically possess any of the symmetries (1.2) except for the identity.

Our results will apply to the subclass LC_0 of systems whose members also generate a smooth local semi-flow on a suitable function space [20–24], as well as some technical conditions which will be specified as we proceed.

The paper is organized as follows. In the second section, we derive the center bundle equations of the semi-flow of a system in LC_0, near a hyperbolic rotating wave. We state and prove our main results in the third section: to wit, spiral anchoring is generic in a parameter wedge. Then, we provide a visual criterion characterizing the anchoring wedges in the case $n = 2$. Finally, we perform numerical experiments demonstrating the validity of our results.

2. Reduction to the Center Bundle Equations

Let X be a Banach space, $\mathcal{U} \subset \mathbb{R}^n$ a neighborhood of the origin and $\Phi_{t,\lambda}$ be a smoothly parameterized family (parameterized by $\lambda \in \mathcal{U}$) of smooth local semi-flows on X.

Let $\mathbb{SE}(2) = \mathbb{C}\dotplus\mathbb{SO}(2)$ denote the group of all planar translations and rotations, and let

$$a : \mathbb{SE}(2) \longrightarrow \mathrm{GL}(X) \qquad (2.1)$$

be a faithful and isometric representation of $\mathbb{SE}(2)$ in the space of bounded, invertible linear operators on X. For example, if X is a space of functions with planar domain, a typical $\mathbb{SE}(2)$ action (such as (1.2) in the preceding section) is given by

$$(a(\gamma)u)(x) = u(\gamma^{-1}(x)), \quad \gamma \in \mathbb{SE}(2).$$

We will parameterize $\mathbb{SE}(2)$ as follows: $\mathbb{SE}(2) \cong \mathbb{C} \times \mathbb{S}^1$, with multiplication given by $(p_1, \varphi_1) \cdot (p_2, \varphi_2) = (e^{i\varphi_1} p_2 + p_1, \varphi_1 + \varphi_2)$, $\forall (p_1, \varphi_1), (p_2, \varphi_2) \in \mathbb{C} \times \mathbb{S}^1$. For fixed $\xi \in \mathbb{C}$, we define the following subgroup of $\mathbb{SE}(2)$:

$$\mathbb{SO}(2)_\xi = \{ (\xi, 0) \cdot (0, \theta) \cdot (-\xi, 0) \mid \theta \in \mathbb{S}^1 \}$$

which is isomorphic to $\mathbb{SO}(2)$, and represents rotations about the point ξ. We will assume the following symmetry conditions on the family $\Phi_{t,\lambda}$ of semi-flows.

Hypothesis 1 *There exists n distinct points $\xi_1, \ldots, \xi_n$ in $\mathbb{C}$ such that if e_j denotes the jth vector of the canonical basis in $\mathbb{R}^n$, then $\forall u \in X, \alpha \neq 0, t > 0$,*

$$\Phi_{t,\alpha e_j}(a(\gamma)u) = a(\gamma)\Phi_{t,\alpha e_j}(u) \iff \gamma \in \mathbb{SO}(2)_{\xi_j}, \quad and$$
$$\Phi_{t,0}(a(\gamma)u) = a(\gamma)\Phi_{t,0}(u), \quad \forall \gamma \in \mathbb{SE}(2).$$

Hypothesis 1 basically states that (a) when $\lambda = 0$, the semi-flow $\Phi_{t,0}$ is $\mathbb{SE}(2)$-equivariant; (b) when $\lambda \neq 0$ is near the origin and along the jth coordinate axis of $\mathbb{R}^n$, the semi-flow is only $\mathbb{SO}(2)_{\xi_j}$-equivariant (i.e. it only commutes with rotations about the point ξ_j), and (c) when λ is not as in (a) or (b), the semi-flow has (generically) trivial equivariance.

We are interested in the effects of the forced symmetry-breaking on normally hyperbolic rotating waves. Therefore, we will assume the following hypothesis.

Hypothesis 2 *There exists $u^* \in X$ and Ω^* in the Lie algebra of $\mathbb{SE}(2)$ such that $e^{\Omega^* t}$ is a rotation and $\Phi_{t,0}(u^*) = a(e^{\Omega^* t})u^*$ for all t. We also assume that the set $\{ \lambda \in \mathbb{C} \mid |\lambda| \geq 1 \}$ is a spectral set for the linearization $a(e^{-\Omega^*})D\Phi_{1,0}(u^*)$ with projection P_* such that the generalized eigenspace $\mathrm{range}(P_*)$ is three dimensional.*

For sake of simplicity, we will only be interested in one-armed spiral waves; therefore, we assume that u^* in hypothesis 2 has trivial isotropy subgroup. While hypotheses 1 and 2 hold for a large variety of spirals (such as decaying spirals), there is also a large family of spirals for which they don't (including Archimedean spirals) [29].§

Let LC_0 be the collection of all abstract dynamical systems that do satisfy them, as well as all other hypotheses required in order for the center manifold theorems of [20–23] to hold, and let $\Phi_{t,\lambda}$ be produced by some member of LC_0. It follows that for λ near the origin in $\mathbb{R}^n$, the essential dynamics of the semi-flow $\Phi_{t,\lambda}$ near the rotating wave reduces

§ However, even in the case of Archimedean spirals (for which hypothesis 1 fails), finite-dimensional center-bundle equations which share the symmetries of the underlying abstract dynamical systems have been shown to possess a definite predictive value in terms of possible dynamics and bifurcations of these spiral waves [1–5].

to the following ordinary differential equations on the bundle $\mathbb{C} \times \mathbb{S}^1$ (see [32] for more details):

$$\dot{p} = e^{i\varphi} V + G^p(p, \overline{p}, \varphi, \lambda)$$
$$\dot{\varphi} = \omega + G^\varphi(p, \overline{p}, \varphi, \lambda) \tag{2.2}$$

where V is a complex constant, $\omega \neq 0$ is a real constant, G^p and G^φ are smooth, uniformly bounded in p, and such that $G^p(p, \overline{p}, \varphi, 0) = 0$ and $G^\varphi(p, \overline{p}, \varphi, 0) = 0$. If λ is near the origin, we can re-scale time along orbits of (2.2) to get

$$\dot{p} = e^{i\varphi} v + \mathcal{G}(p, \overline{p}, \varphi, \lambda)$$
$$\dot{\varphi} = 1 \tag{2.3}$$

where $\mathcal{G}$ is smooth, uniformly bounded in p, and such that $\mathcal{G}(p, \overline{p}, \varphi, 0) \equiv 0$. Of course, $\mathcal{G}$ is not completely arbitrary because of the symmetry conditions in hypothesis 1. A simple computation and Taylor's theorem lead to the following.

Proposition 2.1 *The symmetry conditions in hypothesis 1 imply that the equations (2.3) have the general form*

$$\dot{p} = e^{i\varphi(t)} \left[v + \sum_{j=1}^{n} \lambda_j H_j((p - \xi_j)e^{-i\varphi(t)}, \overline{(p - \xi_j)}e^{i\varphi(t)}, \lambda) \right] \tag{2.4}$$

where, without loss of generality, $\varphi(t) = t$, $v \in \mathbb{C}$, $\lambda = (\lambda_1, \ldots, \lambda_n)$, and the functions H_j are smooth and uniformly bounded in p.

A $2\pi-$periodic solution p_λ of (2.4) is called a *perturbed rotating wave* of (2.4). Define the average value

$$[p_\lambda]_\mathrm{A} = \frac{1}{2\pi} \int_0^{2\pi} p_\lambda(t) \, dt. \tag{2.5}$$

If the Floquet multipliers of p_λ all lie within (resp. outside) the unit circle, we shall say that $[p_\lambda]_\mathrm{A}$ is the *anchoring* (resp. *repelling*, or *unstable anchoring*) *center* of p_λ.

In the following section, we will perform an analysis of anchoring of perturbed rotating waves of (2.4) for parameter values near $\lambda = 0$.

3. Analysis of the Center Bundle Equations

Equations (2.4) represent the dynamics near a normally hyperbolic rotating wave for a parameterized family $\Phi_{t,\lambda}$ of semi-flows satisfying the forced-symmetry breaking conditions in hypothesis 1. We start with a brief review of the case $n = 1$ which was studied in detail in [3], and then present new results on the general n case.

3.1. The Case $n = 1$

In this case, we may assume without loss of generality that $\xi_1 = 0$, so that (2.4) has the form

$$\dot{p} = e^{it}\left[v + \lambda H(pe^{-it}, \overline{p}e^{it}, \lambda)\right] \tag{3.1}$$

where $\lambda \in \mathbb{R}$ is small. By writing $w = pe^{-it} + iv$, this system becomes

$$\dot{w} = -iw + \lambda \widetilde{H}(w, \overline{w}, \lambda) \tag{3.2}$$

where $\widetilde{H}(w, \overline{w}, \lambda) = H(w - iv, \overline{w} + i\overline{v}, \lambda)$. The following theorem is proved in [3].

Theorem 3.1 *Let $a = \mathrm{Re}(D_1\widetilde{H}(0, 0, 0))$, where $\widetilde{H}$ is as in (3.2). If $a \neq 0$, then for all $\lambda \neq 0$ small enough, (3.1) has a hyperbolic rotating wave*

$$p(t) = (-iv + O(\lambda))\, e^{it}, \quad \varphi(t) = t. \tag{3.3}$$

The origin $[p]_A = 0$ is an anchoring center if $a\lambda < 0$; it is a repelling center if $a\lambda > 0$.

Remark 3.2 In the case where the semi-flow $\Phi_{t,\lambda}$ is generated by a system of planar reaction-diffusion partial differential equations, the solution (3.3) represents a wave which is rigidly and uniformly rotating around the origin in the plane. In the case where $a\lambda < 0$, the rotating wave is locally asymptotically stable. When $a\lambda > 0$, the rotating wave is unstable (see [8] for an experimental characterization of this phenomenon in an Oregonator model).

3.2. The Case $n > 1$

One might think that the combination of many perturbations would just combine the effects of each perturbation, so that spirals would be observed anchoring at each of the centers, but we shall see that this is not usually the case.

By re-labeling the indices in (2.4) if necessary, we can temporarily shift our point of view so that ξ_1 plays the central role in the following analysis. Then, under the co-rotating frame of reference $z = p - \xi_1 + ie^{it}v$, (2.4) becomes

$$\dot{z} = \dot{p} - e^{it}v = e^{it}\sum_{j=1}^{n}\lambda_j H_j\big((z - \zeta_j)e^{-it} - iv, \overline{(z - \zeta_j)}e^{it} + i\overline{v}, \lambda\big), \tag{3.4}$$

where $\zeta_j = \xi_j - \xi_1$ for $j = 1, \ldots, n$.

When $\lambda_1 \neq 0$ and $\lambda_2 = \cdots = \lambda_n = 0$, we find ourselves in the situation described in the previous subsection. Now, set $\varepsilon = \lambda_1$, $\mu_1 = 1$ and $\lambda_j = \mu_j\varepsilon$ for $j = 2, \ldots, n$ and

$\mu = (\mu_2, \ldots, \mu_n) \in \mathbb{R}^{n-1}$. Then (3.4) can be viewed as a perturbation of the corresponding equation in the case $n = 1$. Note that $\zeta_1 = 0$ and $\lambda = (1, \mu)\varepsilon$.

Equation (3.4) rewrites as

$$\dot{z} = \varepsilon e^{it} \sum_{j=1}^{n} \mu_j H_j\big((z - \zeta_j)e^{-it} - iv, \overline{(z - \zeta_j)}e^{it} + i\overline{v}, (1, \mu)\varepsilon\big). \tag{3.5}$$

Let $\hat{H}_j(w, \overline{w}, \varepsilon, \mu) = H_j\big(w - iv, \overline{w} + i\overline{v}, (1, \mu)\varepsilon\big)$ for $j = 1, \ldots n$. Then (3.5) becomes

$$\dot{z} = \varepsilon e^{it} K(ze^{-it}, \overline{z}e^{it}, t, \varepsilon, \mu) \tag{3.6}$$

where $K(w, \overline{w}, t, \varepsilon, \mu) = \sum_{j=1}^{n} \mu_j \hat{H}_j(w - \zeta_j e^{-it}, \overline{w} - \overline{\zeta}_j e^{it}, \varepsilon, \mu)$ is $2\pi-$periodic in t.

Set $\alpha_1 = D_1 H_1(-iv, i\overline{v}, 0)$. The time$-2\pi$ map P of (3.6) is given by

$$P(z, \overline{z}, \varepsilon, \mu) = z + 2\pi\varepsilon\Big[\alpha_1 z + O\big(|z|^2\big) + O\big(\varepsilon, \mu_2, \ldots, \mu_n\big)\Big] \tag{3.7}$$

near $z = 0$ and $(\varepsilon, \mu) = (0, 0)$.

Hyperbolic fixed points of (3.7) correspond to hyperbolic $2\pi-$periodic solutions of (3.6), and so to perturbed rotating waves of (2.4), that is, the path traced by the solution wave need not be circular. As $z = 0$ is not generally a fixed point of (3.7), these perturbed rotating waves may not be centered at ξ_1. Indeed, let

$$B(z, \overline{z}, \varepsilon, \mu) = \alpha_1 z + O\big(|z|^2\big) + O\big(\varepsilon, \mu_2, \ldots, \mu_n\big) \tag{3.8}$$

be the function inside the square brackets in (3.7). Note that $B(0, 0, 0, 0) = 0$ and that, generically, $D_1 B(0, 0, 0, 0) = \alpha_1 \neq 0$. By the implicit function theorem, there is a unique smooth function $z(\varepsilon, \mu)$ defined near $(\varepsilon, \mu) = (0, 0)$ with $z(0, 0) = 0$ and

$$B\big(z(\varepsilon, \mu), \overline{z}(\varepsilon, \mu), \varepsilon, \mu\big) \equiv 0 \tag{3.9}$$

near $z = 0$. This leads to the following theorem.

Theorem 3.3 *Let α_1 be as in the preceding discussion, with $\mathrm{Re}(\alpha_1) \neq 0$. If the parameters are small enough to satisfy the conditions outlined in the proof below, the time-2π map (3.7) has a unique family of hyperbolic fixed points, whose stability is exactly determined by the sign of $\varepsilon \, \mathrm{Re}(\alpha_1)$.*

Proof: Let B be as in (3.8) and $z(\varepsilon, \mu)$ be the unique continuous function solving the equation $B = 0$ for small parameter values, as asserted above. When $\varepsilon = 0$, any point of $\mathbb{R}^2$ is a non-hyperbolic fixed point of P and so, from now on, we will assume that

$\varepsilon \neq 0$. If that is the case, and if ε and $\|\mu\|$ are small enough, the eigenvalues $\omega_{1,2}(\varepsilon, \mu)$ of $DP(z(\varepsilon, \mu), \varepsilon, \mu)$ satisfy

$$|\omega_{1,2}(\varepsilon, \mu)|^2 = 1 + 4\pi\varepsilon \operatorname{Re}(\alpha_1) + \varepsilon O(\varepsilon, \mu) \neq 1,$$

since $\operatorname{Re}(\alpha_1) \neq 0$. In other words, the fixed point $z(\varepsilon, \mu)$ is hyperbolic. When $\varepsilon \operatorname{Re}(\alpha_1) < 0$, the eigenvalues lie inside the unit circle and the fixed point is asymptotically stable; otherwise, it is unstable. $\qquad\square$

We are now able to formulate and prove the following result.

Theorem 3.4 *Suppose the hypotheses of theorem 3.3 are satisfied. Then there exists a wedge-shaped region near $\lambda = 0$ of the form*

$$\mathcal{W}_1 = \{(\lambda_1, \ldots, \lambda_n) \in \mathbb{R}^n : |\lambda_j| < W_{1,j}|\lambda_1|, \ W_{1,j} > 0, \ \text{for } j \neq 1 \text{ and } \lambda_1 \text{ near } 0\}$$

such that for all $0 \neq \lambda \in \mathcal{W}_1$, (2.4) has a unique perturbed rotating wave $\mathcal{S}_\lambda^1$, with center $[\mathcal{S}_\lambda^1]_A$ generically away from ξ_1. Furthermore, $[\mathcal{S}_\lambda^1]_A$ is a center of anchoring when $\lambda_1 \operatorname{Re}(\alpha_1) < 0$.

Proof: For $j \neq 1$, let $W_{1,j} > 0$ be such that the conclusion of theorem 3.3 holds for any μ_j with $|\mu_j| < W_{1,j}$. Let $\mathcal{W}_1$ be as stated in the hypothesis. If (ε, μ) is such that the time-2π map (3.7) has a hyperbolic fixed point $z(\varepsilon, \mu)$ near 0, then (3.5) has a hyperbolic $2\pi-$periodic orbit $\tilde{z}_{\varepsilon,\mu}(t)$ centered at a point near $z = \zeta_1 = 0$.
For $j \neq 1$, let $\lambda_1 = \varepsilon \neq 0$ be small enough and set $\lambda_j = \mu_j \varepsilon$. Then $\lambda \in \mathcal{W}_1$, as

$$|\lambda_j| = |\mu_j||\varepsilon| < W_{1,j}|\lambda_1| \quad \text{for } j \neq 1,$$

and $\tilde{z}_{\varepsilon,\mu}(t)$ is a $2\pi-$periodic orbit for the parameter λ, which we denote by $z_\lambda(t)$. Since $p = z - ie^{it}v + \xi_1$, (2.4) has a unique perturbed rotating wave $\mathcal{S}_\lambda^1$, with

$$[\mathcal{S}_\lambda^1]_A = \frac{1}{2\pi} \int_0^{2\pi} \left(z_\lambda(t) - ie^{it}v + \xi_1\right) dt = \xi_1 + [z_\lambda]_A.$$

If $0 \neq \lambda \in \mathcal{W}$ is such that $\mu_j = \lambda_j/\varepsilon \neq 0$ is fixed for $j = 2, \ldots, n$, then $[z_\lambda]_A = O(1)$ as $\lambda_1 \to 0$ and so $[\mathcal{S}_\lambda^1]_A \neq \xi_1$, generically. The conclusion about the stability of $\mathcal{S}_\lambda^1$ follows directly from theorem 3.3. $\qquad\square$

Remark 3.5 When λ approaches the λ_1-axis away from the origin, $[\mathcal{S}_\lambda^1]_A \to \xi_1$. On the other hand, when the parameter values stray outside of $\mathcal{W}_1$, all that can generically be said with certainty is that solutions of (2.4) locally drift away from ξ_1, which cannot then be a center of anchoring. After drifting, the spiral may very well get anchored at some point far from ξ_1, depending on the global nature of the perturbation functions H_j in (2.4).

The preceding results have been achieved by considering (2.4) under a co-rotating frame of reference around ξ_1. Of course, since the choice for ξ_1 was arbitrary, corresponding results must also be achieved, in exactly the same manner, when the viewpoint shifts to another ξ_k. For $j = 1, \ldots, n$, let $\alpha_j = D_1 H_j(-iv, i\overline{v}, 0)$ be the *anchoring coefficients* of (2.4).

Theorem 3.6 *Let $k \in \{1, \ldots, n\}$. If $\mathrm{Re}(\alpha_k) \neq 0$, then there exists a wedge-shaped region near $\lambda = 0$ of the form*

$$\mathcal{W}_k = \{(\lambda_1, \ldots, \lambda_n) \in \mathbb{R}^n \; : \; |\lambda_j| < W_{k,j}|\lambda_k|, \;\; W_{k,j} > 0, \; \text{for } j \neq k \text{ and } \lambda_k \text{ near } 0 \,\}$$

such that for all $0 \neq \lambda \in \mathcal{W}_k$, (2.4) has a unique perturbed rotating wave $\mathcal{S}_\lambda^k$, with center $[\mathcal{S}_\lambda^k]_A$ generically away from ξ_k. Furthermore, $[\mathcal{S}_\lambda^k]_A$ is a center of anchoring when $\lambda_k \, \mathrm{Re}(\alpha_k) < 0$.

Clearly, the remark that appears after the proof of theorem 3.4 still holds.

4. Characterization of Spiral Anchoring $(n = 2)$

In the previous section, we described the (local) behaviour of spiral anchoring in small wedges around the parameter coordinate axes. In this section, we present a fuller characterization of spiral wave anchoring for the case $n = 2$.‖

Let $0 \neq \xi \in \mathbb{R}^2$, $\Lambda_0 = (\lambda_1, 0), \Lambda_\xi = (0, \lambda_2) \in \mathbb{R}^2$ and let $P : \mathbb{R}^2 \times \mathbb{R}^2 \to \mathbb{R}^2$ be a real analytic map with $P(x, 0) = x$, $DP(x, 0) = I_2$ for all $x \in \mathbb{R}^2$, satisfying the following conditions: for $\eta \in \{0, \xi\}$,

(P1) $\exists \omega_* > 0$ such that $P(\eta, \Lambda_\eta) \equiv 0$, for all $||\Lambda_\eta|| < \omega_*$;

(P2) the eigenvalues of $DP(\eta, \Lambda_\eta)$ lie both outside or both inside the unit circle for all $0 \neq ||\Lambda_\eta|| < \omega_*$;

(P3) there is a wedge region w_η surrounding the coordinate axis generated by Λ_η in parameter space (see figure 1) in which P has a (locally) unique manifold $x_\eta(\lambda)$ such that, for all $\lambda \in \mathsf{w}_\eta$,

    (a) $P(x_\eta(\lambda), \lambda) \equiv x_\eta(\lambda)$;
    (b) $x_\eta(\lambda) \to \eta$ as λ approaches the coordinate axis away from the origin;
    (c) $x_\eta(\lambda)$ shares its stability with η in (P2).

When the hypotheses of theorem 3.6 hold, the associated time-2π map (3.7) (viewed in real coordinates) satisfies (P1)$-$(P3). Numerous questions cannot be answered by local analysis alone. For instance:

‖ Most of the analysis can be extended and adapted to the general case $n \geq 2$, but at the cost of substantial algebraic complications.
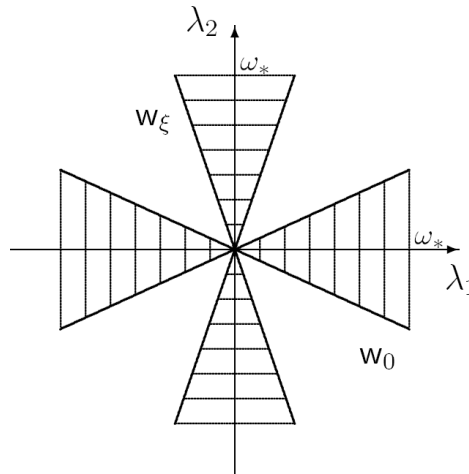
Figure 1. Wedges in parameter space corresponding to property (P3).

(i) Can the wedges overlap? What does that imply for anchoring in (2.4)?

(ii) Can a wedge contain its "opposite" coordinate axis?

(iii) If the wedges do not overlap, what is the nature of their complement?

(iv) If there is a complement with non-trivial measure, what kinds of dynamics can be expected as the parameter vector λ traces a circle around the origin in parameter space?

We will provide answers to these questions by first studying a specific map, then extending our results to the general mapping.

4.1. A Specific Mapping

Consider the mapping $P : \mathbb{R}^2 \times \mathbb{R}^2 \to \mathbb{R}^2$ given by

$$P(x, \lambda) = x + 2\pi \left[\lambda_1 F_0(x) + \lambda_2 G_\xi(x) \right], \tag{4.1}$$

where $0 \neq \xi \in \mathbb{R}^2$, and F_0, G_ξ are real analytic functions of $x, \lambda \in \mathbb{R}^2$.

Such a map is obtained by truncating the $\lambda-$terms of order ≥ 2 from the time-2π map (3.7), for instance. According to theorem 3.6, the jacobians $DF_0(0)$ and $DG_\xi(\xi)$ have a particular structure.

Proposition 4.1 *If $F_0(0) = 0$, $G_\xi(\xi) = 0$, and if*

$$DF_0(0) = \begin{pmatrix} a & -b \\ b & a \end{pmatrix} \quad and \quad DG_\xi(\xi) = \begin{pmatrix} c & -d \\ d & c \end{pmatrix}$$

where $a, c \neq 0$, then there exists $\omega_* > 0$ such that the map defined by (4.1) satisfies the conditions (P1)$-$(P3).

4.1.1. The search for fixed points. Define $A : \mathbb{R}^2 \to \mathbb{M}_2(\mathbb{R})$ by

$$A(x) = \begin{bmatrix} F_0(x) & G_\xi(x) \end{bmatrix}. \tag{4.2}$$

Then, $\hat{x}$ is a fixed point of (4.1) for $\hat{\lambda} \in \mathbb{R}^2$ if and only if $A(\hat{x}) \cdot \hat{\lambda} = 0$, that is if and only if $\hat{\lambda} \in L_{\hat{x}} = \ker A(\hat{x})$. Let $(\hat{x}, \hat{\lambda})$ be such a pair. According to the implicit function theorem, as long as

$$\det \left(D_x P(\hat{x}, \hat{\lambda}) - I \right) = 4\pi^2 \det \left(\hat{\lambda}_1 DF_0(\hat{x}) + \hat{\lambda}_2 DG_\xi(\hat{x}) \right) \neq 0, \tag{4.3}$$

there is a neighbourhood W of $\hat{\lambda}$ and a unique analytic function $X : W \to \mathbb{R}^2$ such that $X(\hat{\lambda}) = \hat{x}$ and $A(X(\lambda)) \cdot \lambda \equiv 0$ for all $\lambda \in W$. By construction, $X(\lambda)$ is a fixed point of (4.1) for all $\lambda \in W$.

If $\dim L_{\hat{x}} = 0$ as a manifold, then $L_{\hat{x}} = \{0\}$. Consequently, the preceding implicit function theorem construction fails, which contradicts property (P3). We need thus only investigate fixed points $\hat{x}$ for which $\dim L_{\hat{x}} \neq 0$. As the quantities under consideration are analytic, it can further be assumed that $\operatorname{rank} A(\hat{x}) = 1$ and $\dim L_{\hat{x}} = 1$.

We now show how to optimally extend the wedge regions w_η using property (P3). Let $(x^*, \lambda_*), (x_*, \lambda_*) \in \mathbb{R}^2 \times (\mathbb{R}^2 - \{0\})$ be such that x^*, x_* are fixed points of (4.1), $\lambda^* \in L_{x^*}, \lambda_* \in L_{x_*}$, and (4.3) is satisfied for both pairs. According to the implicit function theorem, there are open neighbourhoods W^*, W_* of $\lambda^*, \lambda_* \in \mathbb{R}^2$ respectively, and a pair of unique real analytic functions $X^* : W^* \to \mathbb{R}^2$, $X_* : W_* \to \mathbb{R}^2$ for which $X^*(\lambda^*) = x^*$, $X_*(\lambda_*) = x_*$ and

$$A(X^*(\Lambda)) \cdot \Lambda \equiv 0, \text{ for all } \Lambda \in W^*, \quad A(X_*(\Lambda)) \cdot \Lambda \equiv 0, \text{ for all } \Lambda \in W_*.$$

Lemma 4.2 *If $\Lambda_*^* \in W_*^* = W^* \cap W_*$ is such that $X^*(\Lambda_*^*) = X_*(\Lambda_*^*)$, then $X^* = X_*$ on W_*^**

Proof: The assertion follows from the uniqueness of the real analytic functions X^*, X_* in the implicit function theorem. $\square$

Denote the punctured open disc of radius ω_* centered at the origin by $B(0, \omega_*)$. Let $\eta \in \{0, \xi\}$, $\omega_* > 0$ be as in proposition 4.1 and $0 \neq \Lambda_\eta \in \mathsf{w}_\eta$ be a point on the appropriate coordinate axis, as in properties (P1) and (P2). According to these same properties, η is a fixed point of (4.1) for Λ_η and $\det (D_x P(\eta, \Lambda_\eta) - I) \neq 0$.

Lemma 4.2 then implies the existence of a maximal open region W_η, defined as a union of open sets $W \subseteq B(0, \omega_*)$ (in much the same way as the maximal interval is

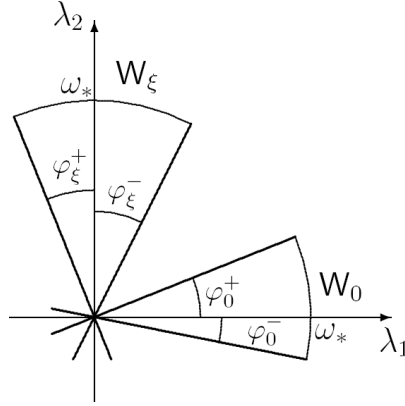**Figure 2.** Wedge angles, with optimal wedge-like regions in parameter space.

built in the Fundamental Theorem of ODE [33]), containing $\mathsf{w}_\eta \cap B(0, \omega_*)$ and for which there is a unique real analytic function $\mathsf{X}_\eta : \mathsf{W}_\eta \to \mathbb{R}^2$ satisfying $x_\eta = \mathsf{X}_\eta|_{\mathsf{w}_\eta}$, where x_η is as in property (P3). Since $\hat{x}$ is a fixed point of (4.1) for $0 \neq \hat{\lambda}$ whenever $\hat{\lambda} \in L_{\hat{x}}$, W_η is described (in polar coordinates) by either one of

$$\mathsf{W}_\eta = \{(r, \theta) : 0 < r < \omega_* \text{ and } s_\eta - \varphi_\eta^- < \theta < s_\eta + \varphi_\eta^+\}$$
$$\mathsf{W}_\eta = \{(r, \theta) : 0 < r < \omega_* \text{ and } \theta \in [0, 2\pi]\}$$

where $\varphi_\eta^-, \varphi_\eta^+ \in (0, \pi/2]$ and

$$s_\eta = \begin{cases} 0 & \text{if } \eta = 0, \\ \pi/2 & \text{if } \eta = \xi. \end{cases}, \tag{4.4}$$

In the latter case, we will say that W_η is *catastrophe-free*. In the former case, the quantities $\varphi_\eta^-, \varphi_\eta^+ \in (0, \pi/2]$ are called the *fore-angle* and *post-angle* of W_η, respectively (see figure 2).

The implicit function theorem fails to extend $A(\mathsf{X}_\eta(\lambda)) \cdot \lambda \equiv 0$ (that is, it fails to extend W_η) at (x^*, λ^*) if either

(C1) $\det\left(\lambda_1^* DF_0(x^*) + \lambda_2^* DG_\xi(x^*)\right) = 0$ and $\mathsf{X}_\eta(\lambda) \to x^*$ as $\lambda \to \lambda^*$, or

(C2) $\|\mathsf{X}_\eta(\lambda)\| \to \infty$ as $\lambda \to \lambda^*$.

Such events will be referred to as *fold* and $\infty-$*catastrophes*, respectively, or *catastrophes*, collectively.

Let $0 < \rho < \omega_*$ and set

$$\gamma_\rho(s) = \rho\left(\cos(s), \sin(s)\right)^\top. \tag{4.5}$$

Assume W_η is not catastrophe-free. Starting at $(\rho, s_\eta) \in \mathsf{W}_\eta$, denote the angles in $(0, \pi/2]$ measuring the first clockwise and the first counter-clockwise occurrence of a catastrophe along γ_ρ by θ_η^- and θ_η^+ respectively. Then, $\varphi_\eta^\pm = s_\eta \pm \theta_\eta^\pm$.

4.1.2. Fold bifurcation points. Modulo a simple regularity condition (see below), (C1) is equivalent to the existence of a fold bifurcation curve in parameter space for (4.1). Indeed, in that case, (x^*, λ^*) is a solution of

$$P(x, \lambda) - x = 0, \qquad \det\left(D_x P(x, \lambda) - I\right) = 0. \tag{4.6}$$

If the (full) Jacobian of the left-hand side of (4.6) has rank 3 at that point, (4.6) has a fold bifurcation curve through λ^* [34]. Such solutions are in one-to-one correspondence with regular solutions of

$$A(x) \cdot \lambda = 0, \qquad \det\left(D_x\left[A(x) \cdot \lambda\right]\right) = 0. \tag{4.7}$$

Set

$$I_{10} = \begin{pmatrix} 1 & 0 \\ 0 & 0 \end{pmatrix}, \quad I_{01} = \begin{pmatrix} 0 & 0 \\ 0 & 1 \end{pmatrix}, \quad \hat{I} = \begin{pmatrix} 0 & 1 \\ 1 & 0 \end{pmatrix}, \quad e_1 = \begin{pmatrix} 1 \\ 0 \end{pmatrix} \quad \text{and} \quad e_2 = \begin{pmatrix} 0 \\ 1 \end{pmatrix},$$

and define $H_1, H_2 : \mathbb{R}^2 \to \mathbb{R}^2$ by

$$H_1(x) = \left[I_{10}A(x) + I_{01}A(x)\hat{I}\right] e_1, \qquad H_2(x) = \left[I_{10}A(x) + I_{01}A(x)\hat{I}\right] e_2.$$

A quick computation shows that (4.7) can be written as

$$A(x) \cdot \lambda = 0, \qquad \lambda^\top Q(x)\lambda = 0, \tag{4.8}$$

where

$$Q(x) = \begin{pmatrix} B(x) & \frac{1}{2}C(x) \\ \frac{1}{2}C(x) & E(x) \end{pmatrix}$$

and

$$\begin{aligned} B(x) &= \det DF_0(x) \\ C(x) &= \det DH_1(x) + \det DH_2(x) \\ E(x) &= \det DG_\xi(x). \end{aligned} \tag{4.9}$$

Let x^* be a fixed point of (4.1) and denote $K_x = \{\lambda : \lambda^\top Q(x)\lambda = 0\}$. Generically, K_{x^*} consists of a single line or a pair of intersecting lines through the origin in parameter space. Writing $\mathsf{L}_x = L_x \cap B(0, \omega_*)$ and $\mathsf{K}_x = K_x \cap B(0, \omega_*)$, we can summarize the situation with the following proposition.

Proposition 4.3 *If (x^*, λ^*) is a regular solution of (4.7) with $\{0\} \neq \mathsf{L}_{x^*} \subseteq \mathsf{K}_{x^*}$, then (x^*, λ) is a fold bifurcation point of (4.1) for all $\lambda \in \mathsf{L}_{x^*}$.*

4.2. The Visual Criterion

Set $\mathfrak{Z} = \{(x, \lambda) : P(x, \lambda) = x \text{ and } \lambda \in \mathsf{L}_x \neq \{0\}\}$ and

$$\kappa(\mathfrak{Z}) = \{x : \exists\, \lambda \neq 0 \text{ such that } (x, \lambda) \in \mathfrak{Z}\}.$$

By construction, $\kappa(\mathfrak{Z})$ is the zero-set of $\det A(x)$ in $\mathbb{R}^2$ and $0, \xi \in \kappa(\mathfrak{Z})$. Generically, $\kappa(\mathfrak{Z})$ is a collection $\mathcal{C}$ of isolated planar curves, whose constituents come in two varieties: bounded or unbounded.¶ Denote this partition by $\mathcal{C} = \mathcal{C}_{\mathrm{B}} \sqcup \mathcal{C}_\infty$ and let C_0, C_ξ be the curves in $\mathcal{C}$ for which $0 \in C_0$ and $\xi \in C_\xi$.

Let $\gamma_\rho : [0, 2\pi] \to \mathbb{R}^2$ be the circle of radius ρ around the origin, parameterized as in (4.5). For each $(x, \lambda) \in \mathfrak{Z}$, define L_x^ρ and K_x^ρ as the intersection of that circle with L_x and K_x, respectively, and let $P_\rho : \mathbb{R}^2 \times [0, 2\pi] \to \mathbb{R}^2$ be given by

$$P_\rho(x, s) = x + 2\pi\rho\big[\cos(s)F_0(x) + \sin(s)G_\xi(x)\big]. \tag{4.10}$$

Then L_x^ρ consists of two antipodal points $\{\pm\alpha_{x,\rho}\}$, and the fixed points (x, s) of P_ρ are in one-to-one correspondence with the 'lines' of fixed points (x, L_x) of P for which $\mathsf{L}_x \neq \{0\}$ (see proposition 4.3).

Set $\mathfrak{Z}_\rho = \{(x, s) \in \mathbb{R}^2 \times [0, 2\pi] : P_\rho(x, s) = x \text{ and } \gamma_\rho(s) \in \mathsf{L}_x^\rho\}$ and

$$\kappa_\rho(\mathfrak{Z}_\rho) = \{x : (x, s) \in \mathfrak{Z}_\rho\}.$$

By construction, $\kappa_\rho(\mathfrak{Z}_\rho) = \kappa(\mathfrak{Z})$. Thus for each $C \in \mathcal{C}$, $\kappa_\rho^{-1}(C)$ is a branch of fixed points in the bifurcation diagram of P_ρ. According to section 4.1.1, the converse also holds: each branch of fixed points in the bifurcation diagram of P_ρ projects down *via* κ_ρ to a curve in $\mathcal{C}$.

The existence and location of fold catastrophes cannot be read directly from $\mathcal{C}$, but the next proposition remedies that situation.

Let $(x^*, \alpha) \in \mathbb{R}^2 \times (\mathbb{R}^2 - \{0\})$ be such that $\|\alpha\| = \rho$, $\alpha \in \mathsf{L}_{x^*}^\rho \subseteq \mathsf{K}_{x^*}^\rho$. Recall that $A(x^*) \neq 0$. Then, $(A_{j,1}(x^*)\ A_{j,2}(x^*)) \neq 0$ for some $j \in \{1, 2\}$ and

$$L_{x^*} = \{\lambda : A_{j,1}(x^*)\lambda_1 + A_{j,2}(x^*)\lambda_2 = 0\}.$$

The function $\Gamma_j : \mathbb{R}^2 \to \mathbb{R}^2$ defined by

$$\Gamma_j(x) = \big[A_{j,2}^2(x)B(x) - A_{j,1}(x)A_{j,2}(x)C(x) + A_{j,1}^2(x)E(x)\big], \tag{4.11}$$

¶ Indeed, were any such curves to intersect at x_*, P would undergo a transcritical bifurcation along $\kappa^{-1}(x_*)$. Such bifurcations are not generically permitted by (C1) and (C2).

where B, C and E are as in (4.9), is called the $j-fold$ *bifurcation function* of (4.1). Let $\mathcal{R}_j$ be the zero-set of $\Gamma_j(x)$ in $\mathbb{R}^2$. We shall say that x^* is a *transverse intersection* of $\kappa(3)$ and $\mathcal{R}_j$ if $\det A(x^*) = \Gamma_j(x^*) = 0$ and

$$\operatorname{rank} D \begin{pmatrix} \det A(x^*) \\ \Gamma_j(x^*) \end{pmatrix} = 2.$$

Proposition 4.4 *Let $j \in \{1,2\}$. If x^* is a transverse intersection of $\kappa(3)$ and $\mathcal{R}_j$ such that $(A_{j,1}(x^*)\ A_{j,2}(x^*)) \neq 0$ and either*

(1) $B(x^*) = 0$ *and* $A_{j,1}(x^*)C(x^*) - A_{j,2}(x^*)E(x^*) = 0$ *or*

(2) $B(x^*) \neq 0$ *and* $C(x^*)^2 - 4B(x^*)E(x^*) \geq 0$,

then P_ρ undergoes a fold catastrophe at (x^*, s^*) for all s^* such that $\gamma_\rho(s^*) = \pm \alpha_{x^*, \rho}$.

Proof: By re-labeling the terms if necessary, we may assume $A_{j,1} \neq 0$. There are then two possibilities.

(i) If $B = 0$ and $A_{j,1}C - A_{j,2}E = 0$, then

$$K_{x^*} = \{\lambda : \lambda_1 \lambda_2 C + \lambda_2^2 E = 0\} = \{\lambda : \lambda_2 = 0 \text{ or } \lambda_1 C + \lambda_2 E = 0\}.$$

(a) If $\lambda_2 = 0$, then $L_{x^*} = \{(\lambda_1, 0) : \lambda_1 A_{j,1} = 0\} = \{0\}$ since $A_{j,1} \neq 0$. But this contradicts the assumption $\dim L_{x^*} = 1$.

(b) If $\lambda_1 C + \lambda_2 E = 0$, then

$$\operatorname{rank} \begin{pmatrix} A_{j,1} & A_{j,2} \\ C & E \end{pmatrix} = 1.$$

(ii) If $B \neq 0$ and $C^2 - 4BE \geq 0$, then

$$K_{x^*} = \left\{ \lambda : \lambda_1 = \frac{-C \pm \sqrt{C^2 - 4BE}}{2B} \lambda_2 \right\}.$$

In this case,

$$
\begin{aligned}
4B\Gamma_j &= (-2A_{j,2}B + A_{j,1}C)^2 - A_{j,1}^2(C^2 - 4BE) \\
&= \left(-2A_{j,2}B + A_{j,1}\left(C + \sqrt{C^2 - 4BE}\right)\right) \\
&\qquad\qquad \cdot \left(-2A_{j,2}B + A_{j,1}\left(C - \sqrt{C^2 - 4BE}\right)\right) = 0
\end{aligned}
$$

and so

$$-\frac{A_{j,2}}{A_{j,1}} = \frac{-C + \sqrt{C^2 - 4BE}}{2B} \quad \text{or} \quad -\frac{A_{j,2}}{A_{j,1}} = \frac{-C - \sqrt{C^2 - 4BE}}{2B}.$$

In either cases, L_{x^*} is contained in K_{x^*}; thus $\{0\} \neq \mathsf{L}_{x^*} \subseteq \mathsf{K}_{x^*}$ and $\{0\} \neq \mathsf{L}_{x^*}^\rho \subseteq \mathsf{K}_{x^*}^\rho$. As x^* is a transverse intersection of $\kappa(3)$ and $\mathcal{R}_j$, it is also a regular solution of (4.8); (x^*, L_{x^*}) then consists of fold bifurcation points of (4.1), according to proposition 4.3. The desired conclusion follows from $\{\pm\alpha_{x^*,\rho}\} = \mathsf{L}_{x^*}^\rho = \mathsf{L}_{x^*} \cap \gamma_\rho$ and from the correspondence between fixed points of P_ρ and 'lines' of fixed points of P. $\qquad\square$

By construction, the bifurcation diagram of P_ρ is $2\pi-$periodic in s. Consequently, elements of $\mathcal{C}_\mathrm{B}$ must be (bounded) loops and elements of $\mathcal{C}_\infty$ must give rise to two $\infty-$catastrophes. Moreover, the number of fold catastrophes on any given $C \in \mathcal{C}_\mathrm{B}$ cannot be odd as C could not be a loop were that the case. Finally, note that catastrophes cannot occur at 0 or ξ as this would contradict (P2) and (P3).

4.3. The Bifurcation Diagrams

Let C_0, C_ξ, s_0 and s_ξ be as defined previously. Set $\eta \in \{0, \xi\}$. By definition, C_η goes through η at $s = s_\eta$. By (P3), the wedges' angles $\varphi_\eta^\pm$ lie in $(0, \pi)$ or $(0, \pi]$ (when they exist), according to whether they record fold or $\infty-$catastrophes, respectively. Set $\nu_1 = \varphi_0^+ + \varphi_\xi^-$ and $\nu_2 = \varphi_0^- + \varphi_\xi^+$. Then W_0 and W_ξ overlap

(i) in all four quadrants if and only if $\nu_1, \nu_2 > \pi/2$;

(ii) in the first and third quadrants if and only if $\nu_1 > \pi/2$ and $\nu_2 \leq \pi/2$, and in the second and fourth quadrants if and only if $\nu_1 \leq \pi/2$ and $\nu_2 > \pi/2$.

If $\nu_j = \pi/2$, the wedges do not overlap but their complement has zero measure in a neighbourhood of the origin. When the wedge angles $\varphi_\eta^\pm$ do not exist, W_η is a deleted neighbourhood of the origin in parameter space.

4.3.1. The case $C_0 \neq C_\xi$ In this instance, it is sufficient to understand the bifurcation diagrams along a single curve: the full picture can then be obtained by combining the diagrams corresponding to C_0 and C_ξ. When $C_\eta \in \mathcal{C}_\mathrm{B}$, there are two (essentially) distinct generic possibilities.

(i) If there is no fold catastrophe along C_η, then the angles $\varphi_\eta^\pm$ do not exist and W_η is catastrophe-free deleted neighbourhood of the origin in parameter space.

(ii) If there are $2k$ fold catastrophes along C_η, $k > 0$, then the angles $\varphi_\eta^\pm$ are well-defined: $s_\eta \mp \varphi_\eta^\pm$ are the $s-$values of the first fold catastrophes occurring respectively *before* and *after* η along C_η.

When $C_\eta \in \mathcal{C}_\infty$, there are two (essentially) distinct generic possibilities.

(i) If there is no fold catastrophe along C_η, then the angles $\varphi_\eta^\pm$ are well defined and $s_\eta \mp \varphi_\eta^\pm$ are the $s-$values of the $\infty-$catastrophes occurring respectively *before* and *after* η via C_η.
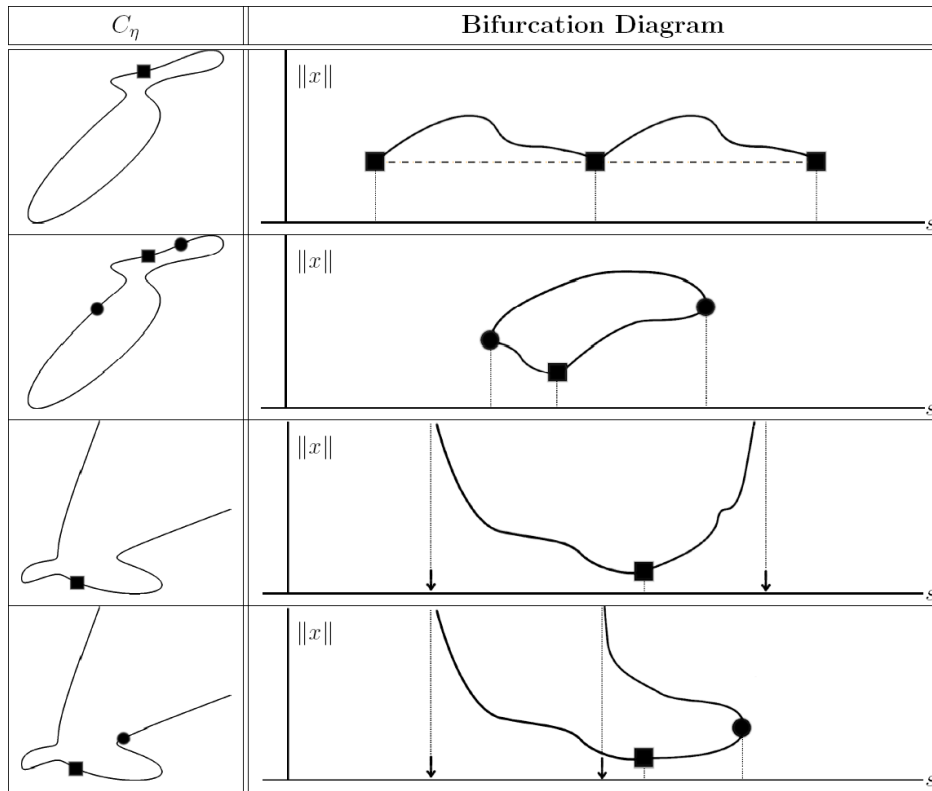
Figure 3. Partial bifurcation diagrams of P_ρ when $C_0 \neq C_\xi$. Only one branch is shown. The square represents the origin or ξ and the circles and arrows indicate fold and ∞-catastrophes, respectively.

(ii) If there are k fold catastrophes along C_η, $k > 0$, then the angles $\varphi_\eta^\pm$ are well-defined: if all the fold catastrophes lie on one side of η (say $s > s_\eta$) along C_η then $s_\eta \mp \varphi_\eta^\pm$ are the s-values of the ∞-catastrophes occurring *before* η and the first fold catastrophe *after* η along C_η, respectively (or *vice-versa*). Otherwise, $s_\eta \mp \varphi_\eta^\pm$ are the s-values of the first fold catastrophes occurring respectively *before* and *after* η along C_η.

Some corresponding qualitative bifurcation diagrams are shown in figure 3.

4.3.2. The case $C_0 = C_\xi$ In this instance, the bifurcation diagram must pass through 0 at $s = 0$ and ξ at $s = \pi/2$. When $C_0 = C_\xi \in \mathcal{C}_B$, the number of fold catastrophes along the curve is even; there are then three (essentially) distinct generic possibilities.

(i) If there is no fold catastrophe along $C_0 = C_\xi$, then the angles $\varphi_0^\pm$ and $\varphi_\xi^\pm$ do not exist and $W_0 = W_\xi$ are catastrophe-free deleted neighbourhoods of the origin in parameter space.

(ii) If there is an odd number of fold catastrophes between the origin and ξ along $C_0 = C_\xi$, then the angles $\mp\varphi_0^\pm$ and $\pi/2 \mp \varphi_\xi^\pm$ are well-defined: they are the $s-$values of the first fold catastrophes occurring respectively *before* and *after* 0 and ξ via $C_0 = C_\xi$.

(iii) If there is an even number of fold catastrophes between 0 and ξ along $C_0 = C_\xi$, the situation is much as described in (2), save for the fact that $C_0 = C_\xi$ is not a loop in the bifurcation diagram of P_ρ.

When $C_0 = C_\xi \in \mathcal{C}_\infty$, there are two (essentially) distinct generic possibilities.

(i) If there is no fold catastrophe along $C_0 = C_\xi$, then the angles $\varphi_0^\pm$ and $\varphi_\xi^\pm$ are well defined and $s_\eta \mp \varphi_\eta^\pm$ are the $s-$values of the $\infty-$catastrophes occurring respectively *before* and *after* 0 and ξ via $C_0 = C_\xi$.

(ii) If there are k fold catastrophes along $C_0 = C_\xi$, $k > 0$, then the angles $\varphi_0^\pm$ and $\varphi_\xi^\pm$ are well-defined: if no fold catastrophe lies between 0 and ξ along $C_0 = C_\xi$ then $\mp\varphi_0^\pm$ and $\pi/2 \mp \varphi_\eta^\pm$ are determined as in the case $C_\eta \in \mathcal{C}_\infty$, item (2) (see p. 18). If there are fold catastrophes between 0 and ξ along $C_0 = C_\xi$, then φ_0^+ and $\pi/2 - \varphi_\xi^-$ are the $s-$values of the first fold catastrophes occurring respectively *after* 0 and *before* ξ along C_ξ.

Some corresponding qualitative bifurcation diagrams are shown in figure 4.

4.4. The General Mapping

The mapping (4.1) is not the most general mapping satisfying (P1)$-$(P3); one should instead study maps of the form

$$\mathcal{P}(x, \lambda) = x + 2\pi\big[\lambda_1\mathcal{F}_0(x, \lambda_1) + \lambda_1\lambda_2\mathcal{J}(x, \lambda) + \lambda_2\mathcal{G}_\xi(x, \lambda_2)\big], \qquad (4.12)$$

where $\xi \neq 0 \in \mathbb{R}^2$, $\mathcal{F}_0$, $\mathcal{J}$ and $\mathcal{G}_\xi$ are real analytic in their variables and the jacobians $D_x\mathcal{F}_0(0, \lambda_1)$ and $D_x\mathcal{G}_\xi(\xi, \lambda_2)$ have the particular form prescribed by proposition 4.5, which is analogous to proposition 4.1.

Proposition 4.5 *If* $\mathcal{F}(0, \lambda_1) \equiv 0$, $\mathcal{G}_\xi(\xi, \lambda_2) \equiv 0$, *and if*

$$D_x\mathcal{F}_0(0, \lambda_1) = \begin{pmatrix} a(\lambda_1) & -b(\lambda_1) \\ b(\lambda_1) & a(\lambda_1) \end{pmatrix} \quad and \quad D_x\mathcal{G}_\xi(\xi, \lambda_2) = \begin{pmatrix} c(\lambda_2) & -d(\lambda_2) \\ d(\lambda_2) & c(\lambda_2) \end{pmatrix},$$

where $a, b, c, d : \mathbb{R} \to \mathbb{R}$ *are continuous in their variables and* $a(0), c(0) \neq 0$, *then there exists* $\omega_* > 0$ *such that the map defined by* (4.12) *satisfies conditions* (P1)$-$(P3).

Define $\mathcal{A} : \mathbb{R}^2 \times \mathbb{R}^2 \to \mathbb{M}_2(\mathbb{R})$ by

$$\mathcal{A}(x, \lambda) = \Big[\mathcal{F}_0(x, \lambda_1) + \tfrac{\lambda_2}{2}\mathcal{J}(x, \lambda) \quad \tfrac{\lambda_1}{2}\mathcal{J}(x, \lambda) + \mathcal{G}_\xi(x, \lambda_2)\Big]; \qquad (4.13)$$
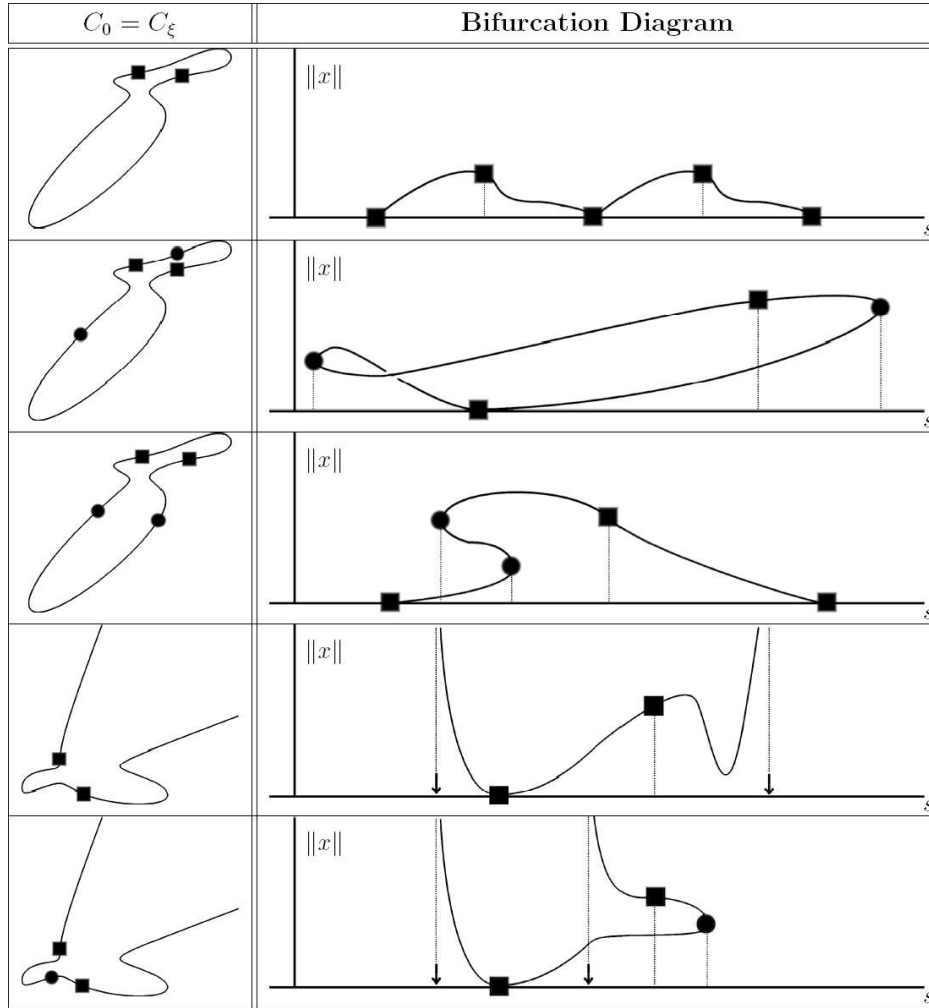
Figure 4. Partial bifurcation diagrams of P_ρ when $C_0 = C_\xi$. The squares represent 0 and ξ, and the circles and arrows indicate fold and ∞−catastrophes, respectively. The apparent self-intersection is an artifact of the projection on the $\|x\| - s$ plane; it does not, in fact, occur.

fixed points of (4.12) are then in one-to-one correspondence with solutions of

$$\mathcal{A}(x, \lambda) \cdot \lambda = 0. \qquad (4.14)$$

Set $\mathfrak{F}(x, \lambda) = \det \mathcal{A}(x, \lambda)$. According to Taylor's theorem, there are appropriate functions K_{10}, K_{01} such that $\mathfrak{F}(x, \lambda) = \mathfrak{F}(x, 0) + \lambda_1 K_{10}(x, \lambda) + \lambda_2 K_{01}(x, \lambda)$.

Let $\hat{x}$ be such that $\mathfrak{F}(\hat{x}, 0) = 0$, $\det D_x \mathfrak{F}(\hat{x}, 0) \neq 0$ and $\mathcal{A}(\hat{x}, 0) \neq 0$. Then, by the implicit function theorem, there is a neighbourhood $\mathfrak{V} \subseteq \mathbb{R}^2$ of the origin and a unique analytic function $\mathfrak{X} : \mathfrak{V} \to \mathbb{R}^2$ such that $\mathfrak{X}(0) = \hat{x}$, $\mathfrak{F}(\mathfrak{X}(\lambda), \lambda) \equiv 0$ and rank $\mathcal{A}(\mathfrak{X}(\lambda), \lambda) = 1 \; \forall \lambda \in \mathfrak{V}$.

Define $\mathfrak{L}_{\hat{x}} = \{\lambda \in \mathfrak{V} : \mathcal{A}(\mathfrak{X}(\lambda), \lambda) \cdot \lambda = 0\}$. A simple rank argument shows that $\mathfrak{L}_{\hat{x}}$ is defined *via* a single equation in two real variables, with a regular solution at the origin; consequently, as a manifold, $\mathfrak{L}_{\hat{x}}$ is one-dimensional.

Let $\mathcal{L}_{\hat{x}} = \ker \mathcal{A}(\hat{x}, 0)$. Then, there is a small neighbourhood $\mathfrak{U} \subseteq B(0, \omega_*)$ of the origin in parameter space for which

$$\{(\mathfrak{X}(\lambda), \lambda) : \lambda \in \mathfrak{U} \cap \mathfrak{L}_{\hat{x}}\} \quad \text{is a deformation of} \quad \{(\hat{x}, \lambda) : \lambda \in \mathfrak{U} \cap \mathcal{L}_{\hat{x}}\} :$$

both 'curves' can be parameterized by the same λ_j, $j = 1, 2$. The preceding discussion shows that the fixed points of (4.12) are in one-to-one correspondence with the fixed points of the (already studied) truncated map

$$\mathcal{P}_{\mathrm{T}}(x, \lambda) = x + 2\pi \big[\lambda_1 \mathcal{F}_0(x, 0) + \lambda_2 \mathcal{G}_\xi(x, 0) \big]. \tag{4.15}$$

Fold bifurcations persist under small perturbations [35, 36]. Similarly, a generic unbounded curve remains unbounded under small perturbations.

Indeed, in the real projective plane, an element of $\mathcal{C}_\infty$ meets the line at infinity in two points. Generically, these two points are distinct and a small perturbation will not change that fact, *i.e* the perturbed curve is still an element of $\mathcal{C}_\infty$. In the non-generic case where the two points at infinity are equal, a small perturbation will either cause the points to separate or to vanish entirely (reminiscent of a fold bifurcation of points at infinity), *i.e* the perturbed curve either stays in $\mathcal{C}_\infty$ or becomes finite.

Thus, catastrophes generically persist: as a result, the bifurcation diagrams of (4.12) and (4.15) are (locally) topologically equivalent for small parameter values λ. Consequently, (4.12) has wedge-like regions $\mathfrak{W}_\eta$ corresponding to the wedge regions W_η of (4.1).

Finally, note that since P is the 'linearization' of $\mathcal{P}$ at the origin with respect to λ, the wedge regions W_η of (4.1) provide tangential 'cones' for the corresponding wedge-like regions $\mathfrak{W}_\eta$ of (4.12).

5. Numerical Simulations and Examples

In this section, we illustrate and interpret the results of the preceding sections through various examples. As such, the emphasis lies with qualitative observations rather than with precise numerical analysis. First, we study systems of PDE from a (naive) numerical perspective: we observe spiral anchoring, as well as hysteresis and homotopy of the spiral tip. Finally, we provide a few examples of mappings of the form (4.12) together with their zero-level sets and partial bifurcation diagrams.

5.1. PDE, FESB and Semi-Flows

In this section, we examine systems of partial differential equations giving rise to semi-flows satisfying the FESB equivariance described in section 2.

Figure 5. Anchoring in (5.1) with perturbations as in (5.2). The spiral tip paths are plotted in black, the anchored perturbed rotating wave is shown in gray, and the squares indicate the location of the perturbation centers.

The computations are carried out on a two-dimensional square domain $[-30, 30]^2$ with 200 grid points to a side and time-step $\Delta t = 0.005$ and Neumann boundary condition, using a 5-point Laplacian and i) an explicit Runge-Kutta 2−stage method of order two in section 5.1.1, and ii) Matsui's fourth-order Runge-Kutta code based on Barkley's `EZ-Spiral` in section 5.1.2. Throughout, centers of anchoring are found *via* fast Fourier transforms of the tip data.

5.1.1. Spiral anchoring Consider the following small perturbation of the FitzHugh-Nagumo equations:

$$u_t = \tfrac{1}{\varsigma}\left(u - \tfrac{1}{3}u^3 - v\right) + \phi_1 + \Delta u,$$
$$v_t = \varsigma(u + \beta - \gamma v - \phi_2), \tag{5.1}$$

where

$$\phi_j(x) = \sqrt{2}\cos(0.05\pi)0.12 f(x_1 - c_{1,j}, x_2 - c_{2,j}), \ j = 1, 2, \tag{5.2}$$

$c_{1,1} = 9$, $c_{2,1} = 0$, $c_{1,2} = -10$, $c_{2,2} = 5\sqrt{3}$ and

$$f(x) = \exp\left(-0.00086\left(x_1^2 + x_2^2\right)\right).$$

Each $g_j(x)$, alone, breaks translational symmetry but preserves rotational symmetry about $(9, 0)$ (for $j = 1$) or $(-10, 5\sqrt{3})$ (for $j = 2$). Note that both perturbations are

uniformly bounded on $\mathbb{R}^2$ and that they go to 0 as $\|x\| \to \infty$. Under these conditions, the flow of (5.1) near a normally hyperbolic rotating wave is equivalent to the flow of some center bundle equation (2.4). Thus, if spiral waves anchor at all, they will generically do so away from either perturbation center. This is confirmed in figure 5, in which the transients anchor at what would be an otherwise unremarkable location.

We now present the results of simulations on a reaction-diffusion system with 4 TSB perturbations. Set

$$
\begin{aligned}
u_t &= \tfrac{1}{\varsigma}\left(u - \tfrac{1}{3}u^3 - v\right) + \phi_1 + \Delta u, \\
v_t &= \varsigma(u + \beta - \gamma v + \phi_2),
\end{aligned}
\tag{5.3}
$$

where $\varsigma = 0.3$, $\beta = 0.6$, $\gamma = 0.5$, and where ϕ_1, ϕ_2 are inhomogeneous terms which depend on $x \in \mathbb{R}^2$ and are defined by

$$
\begin{aligned}
\phi_1(x) &= g_1(x) + g_2(x) = 0.12 f_1(x_1 - 9, x_2) - 0.10 f_2(x_1 + 1, x_2 - 10), \\
\phi_2(x) &= g_3(x) + g_4(x) = -0.12 f_1(x_1 + 10, x_2 - 5\sqrt{3}) + 0.08 f_3(x_1 - 10, x_2 - 10),
\end{aligned}
$$

where $A_1 = 0.12$, $A_2 = -0.10$, $B_1 = -0.12$, $B_2 = 0.08$,

$$
f_j(x) = \exp\left(a_j(x_1^2 + x_2^2)\right), \quad j = 1, 2, 3,
$$

$a_1 = -0.00086$, $a_2 = -0.0008$ and $a_3 = -0.0009$.

Each $g_j(x)$, alone, breaks translational symmetry but preserves rotational symmetry about $c_1 = (9, 0)$ (for $j = 1$), $c_2 = (-1, 10)$ (for $j = 2$), $c_3 = (-10, 5\sqrt{3})$ (for $j = 3$) and $c_4 = (10, 10)$ (for $j = 4$). Note that the four perturbations are uniformly bounded on $\mathbb{R}^2$ and that they go to 0 as $\|x\| \to \infty$. As predicted, anchoring takes place away from the c_j, $j = 1, \ldots, 4$.

The transients in figure 6 appear to first (hyperbolically) approach some manifold along which they travel to the anchored perturbed rotating wave; this will be the topic of an upcoming paper.

5.1.2. Homotopy and hysteresis of rotating waves Following [8], define the modified Oregonator

$$
\begin{aligned}
u_t &= \tfrac{1}{\varsigma}\left(u - u^2 - (fv + \phi)\tfrac{u-q}{u+q}\right) + \Delta u, \\
v_t &= (u - v) + 0.6\Delta v,
\end{aligned}
\tag{5.4}
$$

where $f = 1.4$, $q = 0.002$, $\varsigma = 0.05$ and ϕ is an inhomogeneous term which depends on $x \in \mathbb{R}^2$. When $\phi \equiv 0$, (5.4) has full Euclidean symmetry.
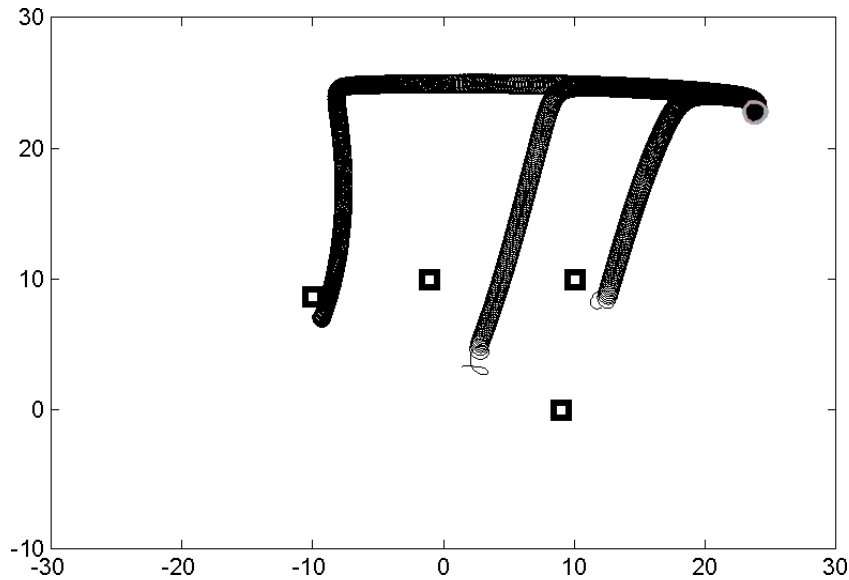
Figure 6. Anchoring in the FitzHugh-Nagumo equations (5.3). The spiral tip paths are plotted in black, the anchored perturbed rotating wave is shown in gray and the black squares indicate the location of the perturbation centers.

In the following simulations, ϕ is the sum of two Gaussian bells:

$$\phi(x) = \alpha_1 \exp\left(-\frac{\|(x_1, x_2) - (15, 15)\|^2}{\beta_1^{\ 2}}\right) + \alpha_2 \exp\left(-\frac{\|(x_1, x_2) - (18.75, 15)\|^2}{\beta_2^{\ 2}}\right),$$

with α_1, α_2, β_1, $\beta_2 \in \mathbb{R}$, and $\beta_1, \beta_2 \neq 0$. Each $g_j(x)$, alone, breaks translational symmetry but preserves rotational symmetry about $c_1 = (15, 15)$ (for $j = 1$) or $c_2 = (18.75, 15)$ (for $j = 2$). Note that both perturbations are uniformly bounded on $\mathbb{R}^2$ and that they go to 0 as $\|x\| \to \infty$.

When $\alpha = (\alpha_1, 0) \neq 0$, (5.4) is $\mathbb{SO}(2)_{c_1}$−equivariant. Similarly, (5.4) is $\mathbb{SO}(2)_{c_2}$−equivariant when $\alpha = (0, \alpha_2) \neq 0$ and trivially equivariant when $\alpha_1, \alpha_2 \neq 0$.

Set $\beta_1 = \beta_2 = 1$ and $\rho_* = 0.01$. Along the path $\alpha(\tau) = \gamma_1(\tau) = \rho_* (\cos(\tau), \sin(\tau))^\top$ in parameter space, (5.4) undergoes a homotopy of perturbed rotating waves, whose tip paths deform continuously from a circle centered at c_1, when $\tau = 0$, to a circle centered at c_2, when $\tau = \pi/2$ (see figure 7).

Along the path $\alpha(\tau) = \gamma_2(\tau) = \frac{1}{10}\gamma_1(\tau)$, however, the homotopy is replaced by hysteresis. As the parameters vary along the path, (5.4) has an anchored perturbed rotating wave whose tip path deforms continuously from a circle centered at c_1. At $\aleph_1 \in \gamma_2$, the rotating wave jumps (discontinuously) to another anchored perturbed rotating wave, whose tip path deforms continuously from a circle centered at c_2.
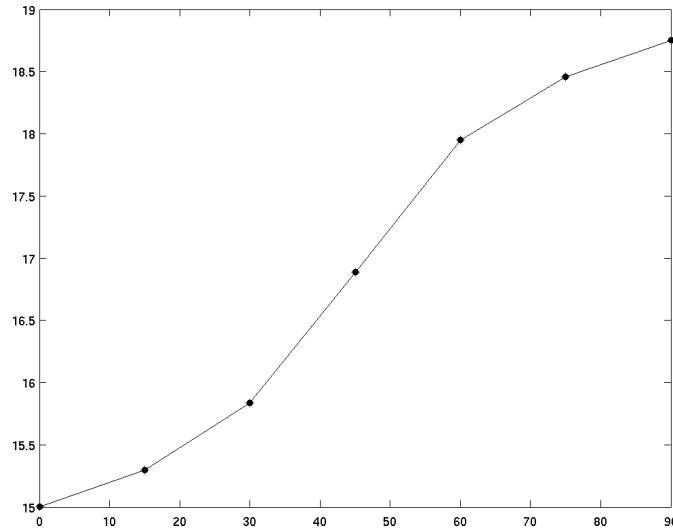
Figure 7. Homotopy of the spiral tip path in (5.4). The first spatial coordinates of the anchoring centers are plotted against τ; compare this image with the first bifurcation diagram on p. 20.

Following γ_2 in the opposite direction leads to similar behaviour, this time with the discontinuous jump taking place at $\aleph_2 \in \gamma_2$, as can be seen in figure 8. Consequently, there must be a third unstable rotating wave (which escapes detection by direct means) appearing and then disappearing at $\aleph_1$ and $\aleph_2$, respectively, in saddle-node bifurcations.

In a sense, both of these occurrences have been predicted by the analysis provided in section 4; consult, for instance, the first and third bifurcation diagrams on p. 20.

5.2. Wedges and Catastrophes

In this final section, we provide a partial catalogue of (partial) bifurcation diagrams for mappings of the form

$$P(x, \lambda) = x + 2\pi \big[\lambda_1 F_0(x) + \lambda_2 G_\xi(x)\big], \tag{5.5}$$

where $\lambda \in \mathbb{R}^2$, $\xi = (2, 2)^\top$,

$$F_0(x) = \begin{pmatrix} 2x_1 - x_2 + \sum a_{i,j} x_1^i x_2^j \\ x_1 + 2x_2 + \sum b_{i,j} x_1^i x_2^j \end{pmatrix} \cdot f_0(x),$$

$$G_\xi(x) = \begin{pmatrix} 7 - 3x_1 - \frac{x_2}{2} + \sum c_{i,j}(x_1 - 2)^i (x_2 - 2)^j \\ 5 - 3x_1 + \frac{x_2}{2} + \sum d_{i,j}(x_1 - 2)^i (x_2 - 2)^j \end{pmatrix} \cdot g_\xi(x),$$

$a_{i,j}, b_{i,j}, c_{i,j}, d_{i,j} \in \mathbb{R}$, $i + j > 1$, and f_0 and g_ξ are continuous functions such that (5.5) satisfies proposition 4.1; we can then use the visual criterion of section 4.2 to under-
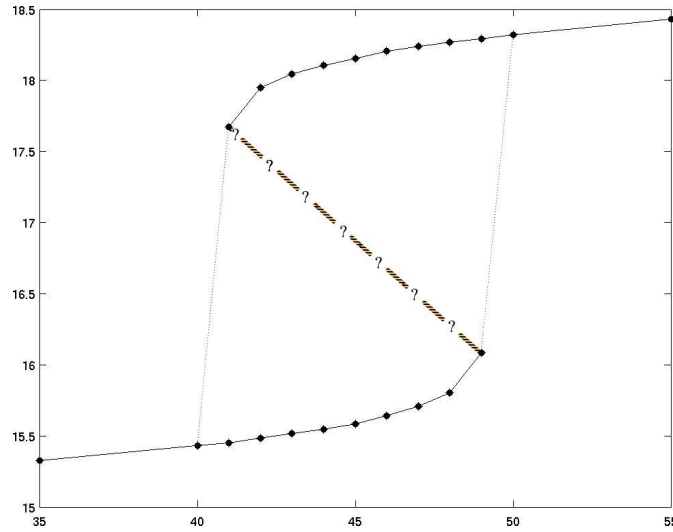
Figure 8. Hysteresis of the spiral tip path in (5.4). The first spatial coordinates of the anchoring centers are plotted against τ. The question marks interpolate (roughly) the unstable rotating waves. Compare this image with the third bifurcation diagram on p. 20.

stand the nature of the bifurcation diagram of the associated map $P_{0.01}$. Furthermore, the wedge angles can be read directly from the bifurcation diagram.

In the figures of this section, C_0 and C_ξ are shown in black or gray. Fold catastrophes are indicated by circles, $\infty-$catastrophes by arrows and the squares mark both the origin and ξ.

5.2.1. The Elowyn-Bonhomme map The Elowyn-Bonhomme (EB) map is obtained from (5.5) by setting $f_0 \equiv g_\xi \equiv 1$, $a_{1,1} = b_{2,0} = c_{0,2} = d_{1,1} = d_{2,0} = 1$, $a_{0,2} = -1$ and all other coefficients to 0; the corresponding $\kappa(\mathbf{3})$ is shown in figure 8. In this instance, $C_0 \in \mathcal{C}_\mathrm{B}$ and $C_\xi \in \mathcal{C}_\infty$. For the EB map, $\omega_* = \frac{12}{37\pi}$. Let $\rho = 0.01 < \omega_*$. Using a pseudo-arc length continuation algorithm (see [37] for details), a partial bifurcation diagram of P_ρ (ignoring all fixed point branches but those through η at $s = s_\eta$, for $\eta \in \{0, \xi\}$) is built: the results can be seen in figure 9.

There are 6 fold catastrophes: two along C_0 and four along C_ξ. Their location can be recovered directly from $\kappa(\mathbf{3})$ and $\mathcal{R}_j$, $j = 1, 2$, with the help of proposition 4.4: in figure 9, the six intersections that satisfy the appropriate hypotheses are marked with circles. Each corresponds to one of the six fold catastrophes observed in figure 7.

Furthermore, two $\infty-$catastrophes occur *via* C_ξ. The interesting values for the EB map are compiled in table 1 above. We continue by providing examples that highlight the various possibilities.

Table 1. EB map catastrophes along C_0 and C_ξ.

Curve	Type	x^*	s^*	Wedge Angle
C_0	Fold	$(1.2483, -0.1286)^\top$	5.9809	$\varphi_0^- \approx 0.3023$
C_0	Fold	$(0.2269, -3.4760)^\top$	0.2308	$\varphi_0^+ \approx 0.2308$
C_ξ	Fold	$(0.3371, 3.1473)^\top$	1.1020	$\varphi_\xi^- \approx 0.4688$
C_ξ	Fold	$(2.2769, 0.2982)^\top$	2.1125	$\varphi_\xi^+ \approx 0.5417$
C_ξ	Fold	$(-3.2933, 6.1024)^\top$	1.1581	n.a.
C_ξ	Fold	$(5.6733, -1.2807)^\top$	1.9267	n.a.
C_ξ	Infinity	n.a.	1.0172	n.a.
C_ξ	Infinity	n.a.	2.3562	n.a.
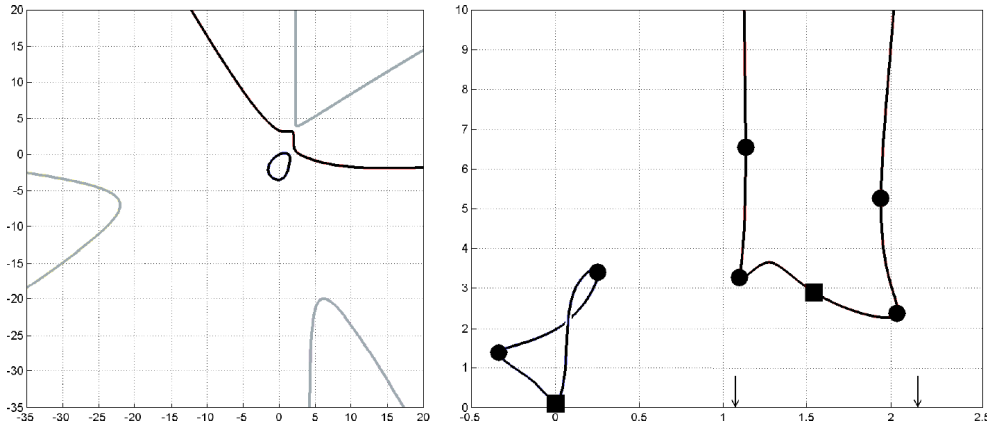
Figure 9. On the left: zero-level set $\kappa(3)$ for the EB map. On the right: fixed point branches of $P_{0.01}$ (the apparent self-intersection on C_0 is due to a projection onto the $\|x\| - s$ plane). Both C_0 (the curve through 0) and C_ξ (the curve through ξ) are shown in black.

5.2.2. The first example

$$a_{2,0} = 0 \qquad a_{1,1} = 1 \qquad a_{0,2} = -1 \qquad b_{2,0} = 1 \qquad b_{1,1} = 0 \qquad b_{0,2} = 0$$

$$c_{2,0} = 0 \qquad c_{1,1} = 0 \qquad c_{0,2} = 1 \qquad d_{2,0} = 1 \qquad d_{1,1} = 1 \qquad d_{0,2} = 0$$

$$f_0(x) = \exp\left(-(x_1^2 + x_2^2)/10\right) \qquad g_\xi(x) = \exp\left(-\left((x_1 - 2)^2 + (x_2 - 2)^2\right)/14\right).$$

See figure 11 for a portion of $\kappa(3)$ and a partial bifurcation diagram of $P_{0.01}$. By construction, the zero-level set for this first example is exactly the zero-level set of the EB map; however, their bifurcation diagrams are not topologically equivalent (compare with figure 9). In this instance, the wedge angles record fold catastrophes on C_0 (black) $\in \mathcal{C}_B$ and $\infty-$catastrophes on C_ξ (gray) $\in \mathcal{C}_\infty$. Note further that this map provides an instance when the anchoring wedges overlap.
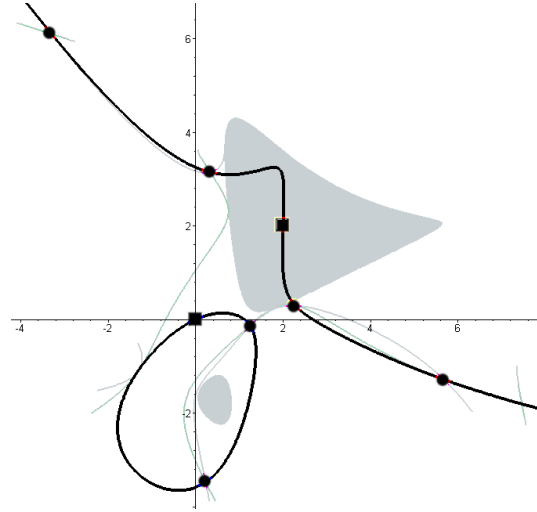
Figure 10. Intersections of the zero-level sets $\kappa(\mathfrak{z})$ (thick black lines) and $\mathcal{R}_1$ and $\mathcal{R}_2$ (thin gray lines) of the Elowyn-Bonhomme problem. The squares represent 0 and ξ; the points that satisfy the hypotheses of proposition 4.4 are marked with circles. The light gray region is part of the planar set for which $C(x)^2 - 4B(x)E(x) < 0$.
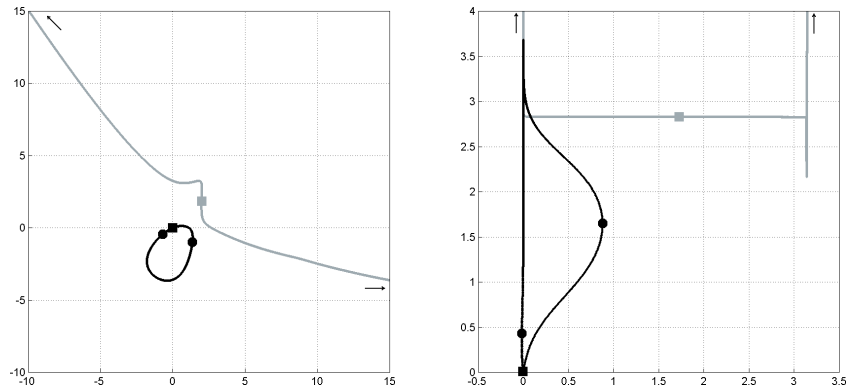

Figure 11. The first example: $\kappa(\mathfrak{z})$ (left), bifurcation diagram of $P_{0.01}$ (right).

5.2.3. The second example

$$a_{2,0} = \frac{2}{5} \qquad a_{1,1} = \frac{43}{10} \qquad a_{0,2} = -\frac{17}{2} \qquad b_{2,0} = \frac{51}{10} \qquad b_{1,1} = -\frac{91}{10} \qquad b_{0,2} = -\frac{12}{5}$$

$$c_{2,0} = -\frac{16}{5} \qquad c_{1,1} = -\frac{99}{10} \qquad c_{0,2} = -\frac{48}{5} \qquad d_{2,0} = -\frac{53}{10} \qquad d_{1,1} = \frac{61}{10} \qquad d_{0,2} = -\frac{99}{10}$$

$$f_0(x) = 1 \qquad g_\xi(x) = 1$$

See figure 12 for a portion of $\kappa(\mathfrak{z})$ and a partial bifurcation diagram of $P_{0.01}$. In this instance, C_0 (black), C_ξ (gray) $\in \mathcal{C}_\infty$, and $\varphi_0^\pm, \varphi_\xi^-$ record fold catastrophes while φ_ξ^+ records an ∞-catastrophe.
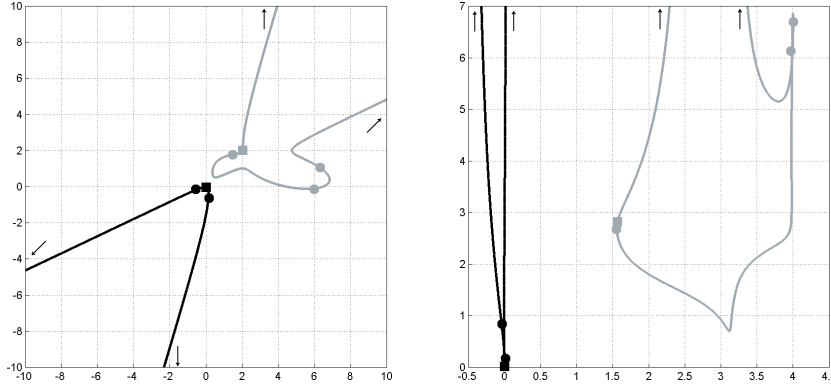
Figure 12. The second example: $\kappa(3)$ (left), bifurcation diagram of $P_{0.01}$ (right).

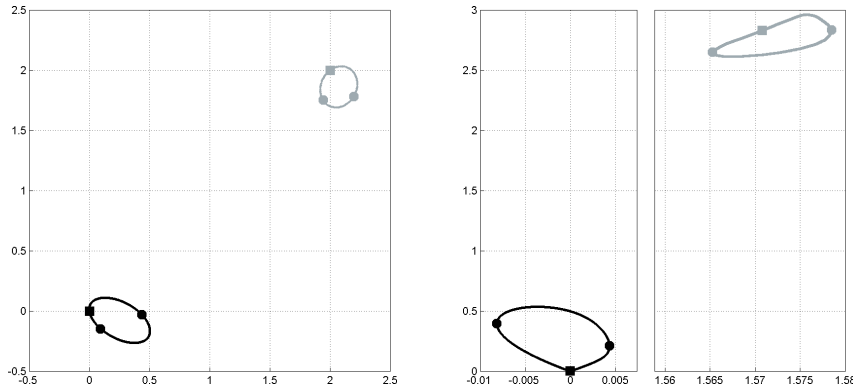**Figure 13.** The third example: $\kappa(3)$ (left), bifurcation diagram of $P_{0.01}$ (right).

5.2.4. The third example

$$a_{2,0} = -\frac{53}{10} \qquad a_{1,1} = -\frac{28}{5} \qquad a_{0,2} = -9 \qquad b_{2,0} = -\frac{9}{5} \qquad b_{1,1} = -\frac{41}{10} \qquad b_{0,2} = -\frac{57}{10}$$

$$c_{2,0} = \frac{22}{5} \qquad c_{1,1} = \frac{21}{5} \qquad c_{0,2} = -\frac{3}{2} \qquad d_{2,0} = -9 \qquad d_{1,1} = \frac{49}{10} \qquad d_{0,2} = -10$$

$$f_0(x) = 1 \qquad g_\xi(x) = 1$$

See figure 13 for a portion of $\kappa(3)$ and a partial bifurcation diagram of $P_{0.01}$. In this instance, C_0 (black), C_ξ (gray) $\in \mathcal{C}_\mathrm{B}$, and the wedge angles all record fold catastrophes.

5.2.5. The fourth example

$$a_{2,0} = 2 \qquad a_{1,1} = \frac{13}{5} \qquad a_{0,2} = -\frac{13}{10} \qquad b_{2,0} = \frac{16}{5} \qquad b_{1,1} = -\frac{21}{10} \qquad b_{0,2} = \frac{3}{5}$$

$$c_{2,0} = -\frac{4}{5} \qquad c_{1,1} = -\frac{3}{10} \qquad c_{0,2} = -\frac{29}{10} \qquad d_{2,0} = -\frac{9}{10} \qquad d_{1,1} = \frac{7}{10} \qquad d_{0,2} = -\frac{3}{2}$$
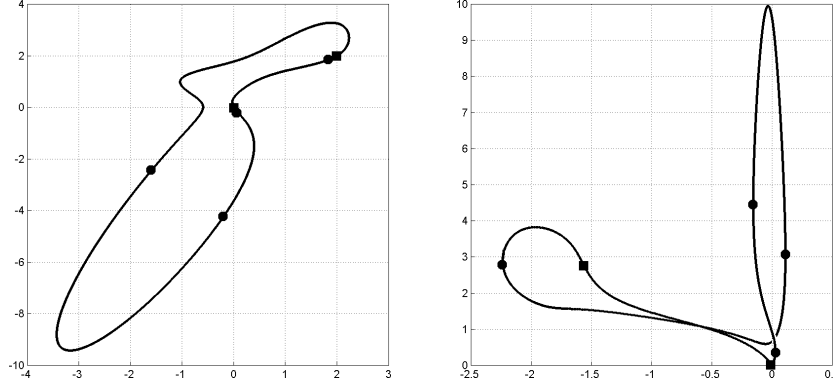
$$f_0(x) = 1 \qquad g_\xi(x) = 1$$

Figure 14. The fourth example: $\kappa(\mathfrak{z})$ (left), bifurcation diagram of $P_{0.01}$ (right).
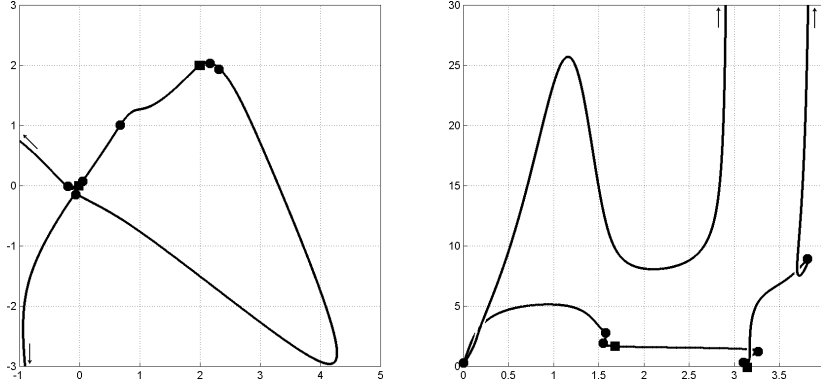

Figure 15. The fifth example: $\kappa(\mathfrak{z})$ (left), bifurcation diagram of $P_{0.01}$ (right).

See figure 14 for a portion of $\kappa(\mathfrak{z})$ and a partial bifurcation diagram of $P_{0.01}$. In this instance, $C_0 = C_\xi \in \mathcal{C}_\mathrm{B}$, the wedge angles all record fold catastrophes and the anchoring wedges overlap.

5.2.6. The fifth example

$$
\begin{array}{lllllll}
a_{2,0} = \frac{59}{10} & a_{1,1} = \frac{43}{10} & a_{0,2} = -7 & a_{3,0} = \frac{38}{5} & a_{2,1} = \frac{27}{5} & a_{1,2} = -\frac{59}{10} & a_{0,3} = -\frac{1}{5} \\
b_{2,0} = -\frac{37}{5} & b_{1,1} = -\frac{51}{10} & b_{0,2} = -\frac{9}{5} & b_{3,0} = \frac{63}{10} & b_{2,1} = \frac{41}{10} & b_{1,2} = -4 & b_{0,3} = \frac{43}{10} \\
c_{2,0} = \frac{11}{5} & c_{1,1} = -\frac{36}{5} & c_{0,2} = -\frac{38}{5} & c_{3,0} = -\frac{61}{10} & c_{2,1} = 2 & c_{1,2} = -\frac{4}{5} & c_{0,3} = -\frac{8}{5} \\
d_{2,0} = -\frac{49}{10} & d_{1,1} = -\frac{38}{5} & d_{0,2} = \frac{27}{10} & d_{3,0} = -\frac{79}{10} & d_{2,1} = \frac{69}{10} & d_{1,2} = -\frac{29}{5} & d_{0,3} = -\frac{41}{10}
\end{array}
$$

$$
f_0(x) = 1 \qquad g_\xi(x) = 1
$$

See figure 15 for a portion of $\kappa(\mathfrak{z})$ and a partial bifurcation diagram of $P_{0.01}$. In this instance, $C_0 = C_\xi \in \mathcal{C}_\infty$ and the wedge angles all record fold catastrophes.
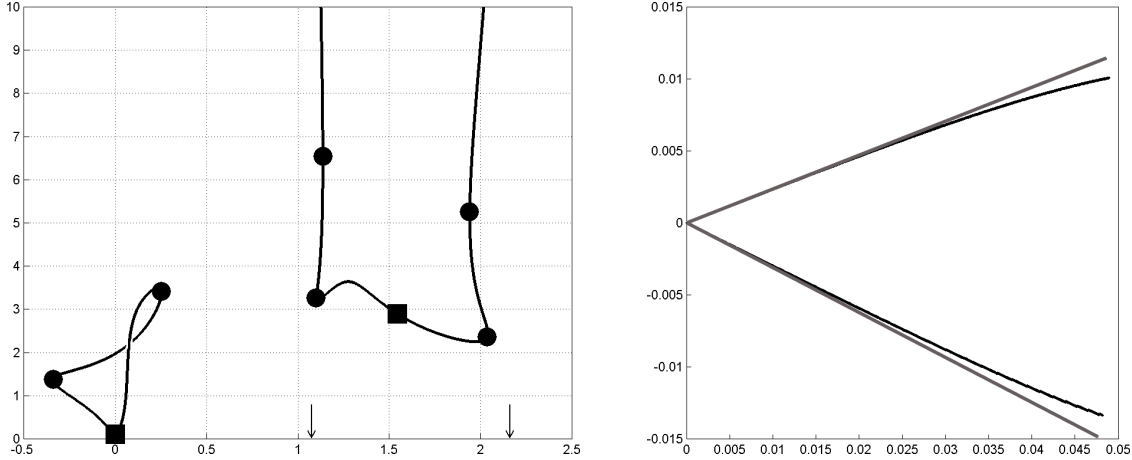
Figure 16. Fixed point branches of $\mathcal{P}_{0.01}$ (left); anchoring wedges W_0 (gray) and $\mathfrak{W}_0$ (black) for the Elowyn-Bonhomme maps (right).

5.2.7. The Elowyn-Bonhomme map revisited Let ξ, F_0 and G_ξ be as in the original EB map (see p. 26) and consider the map $\mathcal{P}$ defined *via* (4.12), with

$$\mathcal{F}_0(x, \lambda_1) = F_0(x) + \lambda_1 \begin{pmatrix} -\frac{28}{5}x_1 + 9x_2 - \frac{9}{5}x_1^2 - \frac{41}{10}x_1x_2 - \frac{57}{10}x_2^2 \\ -9x_1 - \frac{28}{5}x_2 - 9x_1^2 + \frac{49}{10}x_1x_2 - 10x_2^2 \end{pmatrix},$$

$$\mathcal{G}_\xi(x, \lambda_2) = G_\xi(x) + \lambda_2 \begin{pmatrix} 28 - 26x_1 + \frac{2}{5}x_2 + \frac{19}{2}x_1^2 - \frac{33}{10}x_1x_2 - \frac{2}{5}x_2^2 \\ \frac{2}{5} - \frac{38}{5}x_1 - 6x_2 + \frac{28}{5}x_1^2 - \frac{7}{2}x_1x_2 + \frac{23}{5}x_2^2 \end{pmatrix}$$

and

$$\mathcal{J}(x, \lambda) = \begin{pmatrix} \frac{67}{10} + \frac{32}{5}x_1 + \frac{18}{5}x_2 - \frac{33}{5}x_1^2 - x_1x_2 - \frac{8}{5}x_2^2 \\ \frac{59}{10} + \frac{31}{5}x_1 - \frac{46}{5}x_2 + \frac{5}{2}x_1^2 + \frac{79}{10}x_1x_2 + \frac{73}{10}x_2^2 \end{pmatrix}.$$

Then, according to proposition 4.5, $\mathcal{P}$ satisfies (P1)$-$(P3). By the preceding discussion, the bifurcation diagrams of the EB map P is topologically equivalent to that of $\mathcal{P}$ when λ is close enough to the origin.

As an example, let $0.01 < \omega_* = \frac{12}{37\pi}$ and define $\mathcal{P}_{0.01}$ as the restriction of $\mathcal{P}$ to the circle $\gamma_{0.01}(s) = 0.01\,(\cos(s), \sin(s))^\top$ in parameter space. Compare the diagram shown (on the left) in figure 16 with the corresponding diagram of section 5.2.1.

Finally, the wedge regions W_0 of the EB map and $\mathfrak{W}_0$ of the revisited EB map are shown (on the right) in figure 16, illustrating the last remark of section 4.

References

[1] Barkley D 1992 Linear stability analysis of rotating spiral waves in excitable media *Phys. Rev. Lett.* **68** 2090–3

[2] Barkley D 1994 Euclidean symmetry and the dynamics of rotating spiral waves *Phys. Rev. Lett.* **76** 164–7

[3] LeBlanc V G and Wulff C 2000 Translational symmetry-breaking for spiral waves *J. Nonlin. Sc.* **10** 569–601

[4] LeBlanc V G 2002 Rotational symmetry-breaking for spiral waves *Nonlinearity* **15** 1179–203

[5] Li G, Ouyang Q, Petrov V and Swinney H L 1996 Transition from simple rotating chemical spirals to meandering and traveling spirals *Phys. Rev. Lett.* **77** 2105–9

[6] Grill S, Zykov V S and Müller S C 1996 Spiral wave dynamics under pulsatory modulation of excitability *J. Phys. Chem.* **100** 19 082–8

[7] Zykov V S and Müller S C 1996 Spiral waves on circular and spherical domains of excitable medium *Physica D* **97** 322–32

[8] Muñuzuri A P, Pérez-Muñuzuri V and Pérez-Villar V 1998 Attraction and repulsion of spiral waves by localized inhomogeneities in excitable media *Phys. Rev. E* **58** R2689–92

[9] Wiener N and Rosenblueth A 1946 The mathematical formulation of the problem of conduction of impulses in a network of connected excitable elements, specifically in cardiac muscle *Arch. Inst. Card. De Mexico* **16** 205–65

[10] Yermakova Y A and Pertsov A M 1987 Interaction of rotating spiral waves with a boundary *Biophys.* **31** 932–40

[11] Davidenko J M, Persov A V, Salomonsz R, Baxter W and Jalife J 1992 Stationary and drifting spiral waves of excitation in isolated cardiac muscle *Nature* **355** 349–51

[12] Roth B J 1998 Frequency locking of meandering spiral waves in cardiac tissue *Phys. Rev. E* **57** R3735–8

[13] Witkowski F X, Leon L J, Penkoske P A, Giles W R, Spanol M L, Ditto W L and Winfree A T 1998 Spatiotemporal evolution of ventricular fibrillation *Nature* **392** 78–82

[14] Jalife J 2000 Ventricular fibrillation: Mechanisms of initiation and maintenance *Annu. Rev. Physiol.* **62** 25–50

[15] Mackenzie D 2004 Making sense of a heart gone wild *Science* **303** 786–7

[16] Barkley D, Kness M and Tuckerman L S 1990 Spiral-wave dynamics in a simple model of excitable media: The transition from simple to compound rotation *Phys. Rev. Lett.* **42** 2489–92

[17] Winfree A T 1995 in Zipes and Jalife (eds.) *Cardiac Electrophysiology, From Cell to Bedside* second edition (Philadelphia: Saunders) pp. 379–89

[18] Keener J and Sneyd J 1998 *Mathematical Physiology* IAM (New York: Springer)

[19] Barkley D and Kevrekedis I G 1994 A dynamical system approach to spiral wave dynamics *Chaos* **4** 453–60

[20] Sandstede B, Scheel A and Wulff C 1997 Center manifold reduction for spiral waves *C. R. Acad. Sci.* **324** 153–8

[21] Sandstede B, Scheel A and Wulff C 1997 Dynamics of spiral waves on unbounded domains using center-manifold reductions *J. Diff. Eq.* **141** 122–49

[22] Sandstede B, Scheel A and Wulff C 1999 Bifurcations and dynamics of spiral waves *J. Nonlin. Sc.* **9** 439–78

[23] Sandstede B, Scheel A and Wulff C 1999 Dynamical behavior of patterns with euclidean symmetry in Golubitsky, Luss and Strogatz (eds.) *Pattern Formation in Continuous and Coupled Systems* (Berlin: Springer-Verlag)

[24] Fiedler B, Sandstede B, Scheel A and Wulff C 1996 Bifurcation from relative equilibria of noncompact group actions: Skew products, meanders and drifts *Doc. Math.* **1** 479–555

[25] Roth B J 1997 Approximate analytical solutions to the bidomain equations with unequal anisotropy ratios *Phys. Rev. E* **55** 1819–26

[26] Boily P [arXived] Spiral waves and the dynamical system approach

[27] Boily P [forthcoming] Epicyclic drifting in media with multiple inhomogeneities: a dynamical system approach

[28] Boily P [forthcoming] Spiral wave dynamics under combined translational and rotational symmetry-breaking: a dynamical system approach

[29] Scheel A 1998 Bifurcation to spiral waves in reaction-diffusion systems *SIAM J. Math. Anal.* **29** 1399–418

[30] Wulff C 1996 *Theory of Meandering and Drifting Spiral Waves in Reaction-Diffusion Systems* Ph.D. thesis Freie Universität Berlin

[31] Dym H and McKean H P 1972 *Fourier Series and Integrals* (New York: Academic Press)

[32] Boily P 2006 *Spiral Wave Dynamics Under Full Euclidean Symmetry-Breaking: A Dynamical System Approach* Ph.D. thesis University of Ottawa

[33] Hircsh M W and Smale S 1974 *Differential Equations, Dynamical Systems, and Linear Algebra* (San Diego: Academic Press)

[34] Kuznetsov Yu 1995 *Elements of Applied Bifurcation Theory* (Berlin: Springer-Verlag)

[35] Guckenheimer J and Holmes P 1983 *Nonlinear Oscillations, Dynamical Systems, and Bifurcations of Vector Fields* (New York: Springer)

[36] Wiggins S 1990 *Introduction to Applied Non-Linear Dynamical Systems and Chaos* (New York: Springer)

[37] Keller H B 1977 Numerical solutions of bifurcation and nonlinear eigenvalue problems in *Applications of Bifurcation Theory* pp. 359–84